# Does the coupling of the ~~mesospheric~~ semiannual oscillation with the quasi-biennial oscillation provide predictability of Antarctic sudden stratospheric warmings?

Viktoria J. Nordström[1] and Annika Seppälä[1]

[1]Department of Physics, University of Otago, Dunedin, New Zealand

**Correspondence:** Annika Seppälä (annika.seppala@otago.ac.nz)

**Abstract.** During September 2019 ~~there was a~~ a minor sudden stratospheric warming ~~over Antarctica, which brought~~ took place over the Southern Hemisphere (SH), bringing disruption to the usually stable winter vortex. The mesospheric winds reversed and temperatures in the stratosphere rose by over 50 K. Whilst ~~this was only the second~~ SSW in the ~~Southern Hemisphere (SH ), the other~~ SH are rare, with the only major SSW having occurred in 2002, ~~its Northern counterpart~~ the Northern Hemisphere experiences about six per decade. ~~Currently, an amplification~~ Amplification of atmospheric waves during winter is thought to ~~trigger SSWs~~be one of the possible trigger SSWs, although other mechanisms are also possible. Our understanding, however, remains incomplete, especially with regards to ~~its~~ SSW occurrence in the SH. Here, we investigate the ~~interaction~~ effect of two equatorial atmospheric modes, the Quasi Biennial Oscillation (QBO) at 10 hPa and the Semiannual Oscillation (SAO) at 1 hPa during the SH winters of 2019 and 2002. Using MERRA-2 reanalysis data we find that the ~~two modes interact~~ easterly wind patterns resembling the two modes merge at low latitudes ~~during their easterly phases~~ in the early winter, forming a zero wind line that stretches from the lower stratosphere into the mesosphere. This influences the meridional wave guide, resulting in easterly momentum being deposited in the ~~mesosphere~~ polar atmosphere throughout the polar winter, ~~reducing the magnitude of the westerly winds~~ decelerating the westerly winds in the equatorward side of the polar vortex. As the winter progresses~~these features descend~~ , the momentum deposition and wind anomalies descend further down into the stratosphere~~, until SSW conditions are reached~~. We find similar behaviour in ~~two other years leading to delayed dynamical disruptions later in the spring. The timing and~~ other years with early onset SH vortex weakening events. The magnitude of the SAO and the ~~extent~~ timing of the upper stratospheric (10 hPa) easterly QBO signal, ~~that results in the SAO-QBO interaction,~~ was found to be unique in these years, when compared to the years with a similar QBO phase. We were able to identify the SSW/weak vortex years from the early winter location of the zero wind line at 1 hPa together with Eliassen-Palm flux divergence in the upper stratosphere at 40°S-50°S. We propose that this early winter behaviour ~~may be a key physical process in decelerating the mesospheric winds which~~ resulting in deceleration of the polar winds may precondition the Southern atmosphere for a ~~SSW~~later enhanced wave forcing from the troposphere, resulting in a SSW/vortex weakening event. Thus the early winter equatorial upper stratosphere-mesosphere together with the polar ~~mesosphere may provide critical~~ upper atmosphere may provide early clues to an imminent SH SSW.

## 1 Introduction

During the austral winter of 2019, the Southern Hemisphere ~~(SH) experienced a rare atmospheric disruption known as a~~ experienced a minor sudden stratospheric warming (SSW) ~~(for a recent comprehensive review on SSWs see Baldwin et al., 2021)~~ (for a recent comprehensive review on SSWs see Baldwin et al., 2021, and references therein): Between September 5-11 temperatures in the Antarctic stratosphere at 10 hPa warmed by 50 K (Yamazaki et al., 2020). Furthermore, the polar ~~mesospheric~~ zonal mean zonal winds reversed, and the easterlies around 60°S at 10 hPa reached ~60 ~~m/s~~ $ms^{-1}$ around September 16 (Rao et al., 2020c). The ~~SSW's aftermath~~ drivers of this minor SSW have been attributed to enhanced stationary planetary wave activity (Yamazaki et al., 2020).

The impacts of SSWs can influence the atmosphere from the polar region to mid-latitudes for months (see e.g. Baldwin and Dunkerton, 2 . For example, SSWs contribute to the size of the ozone hole via two different mechanisms. First, the warming of the stratosphere suppresses the formation of polar stratospheric clouds (Shen et al., 2020), which play a critical part in stratospheric ozone depletion (Solomon, 1999). Furthermore, the weakening of the vortex allows the mixing of ozone rich mid-latitude air into the pole. Both these effects in combination lead to a smaller ozone hole (Solomon et al., 1986). The anomalous winds from SSWs can also influence stratosphere-troposphere coupling, impacting the Southern and Northern Annular Modes (SAM and NAM) (Taguchi and Hartmann, 2005; Shen et al., 2020; Baldwin et al., 2021; Rao et al., 2020a).

In 2019, the SSW's influence cascaded down through the atmosphere for months following its occurrence. The ~~2019~~ minor SSW pushed the ~~Southern Annual Mode (SAM )~~ SAM into a negative phase (Rao et al., 2020c), ~~which signifies~~ signifying a shift of polar westerlies towards the equator (Doddridge and Marshall, 2017). This movement of strong westerly winds is believed to have impacted the Australian wildfires, which began in the following November (Lim et al., 2019). Furthermore, the changes in polar temperatures and winds shrunk the ozone hole to its smallest size ever observed (Eswaraiah et al., 2020a).

Most of our understanding about SSWs comes from their occurrence over ~~the Arctic,~~ in the Northern Hemisphere (NH), where they take place almost every other year (Charlton and Polvani, 2007). ~~This latest SH SSW is only one of two that has occurred since record keeping began (Rao et al., 2020c), and~~ Due to the rarity of SH SSW events (Rao et al., 2020c), the 2019 case provides a unique opportunity to investigate the ~~triggers of SH SSWs.~~ atmospheric conditions leading up to SH SSWs.

~~As winter descends on the pole, the increase in the meridional temperature gradient accelerates the westerly winds into a vortex (Brasseur, 2005). This isolates the polar air, trapping ozone destroying chemicals, causing the ozone hole over Antarctica (Solomon, 1999), and more recently during strong Northern Hemisphere vortex events, also over the Arctic (Manney et al., 2020; Wohltman . The vortex dissipates in the spring as the atmospheric temperatures warm, in an event known as the final warming (Schoeberl and Newman, . However, during a sudden stratospheric warming the vortex breaks up earlier than expected. Within days of the SSW's onset the vortex weakens, becomes contorted and can break up (Holton, 2012). There is a large-scale warming of the polar stratosphere, which can result in a reversal of the meridional temperature gradient, creating an easterly zonal wind (Volland, 1988) . The World Meteorological Organization (WMO) separates SSWs into two types, major and minor (Charlton and Polvani, 2007) . It should be noted that these definitions are based on Northern Hemisphere (NH) SSW events (Butler et al., 2015). Major events occur when the mean zonal winds at 60° latitude and 10 hPa reverse, and the stratospheric temperature increases, often~~

between 30-50 K (Volland, 1988). Minor events have similar temperature changes to major warmings, however, there is no wind reversal at 60° latitude and 10 hPa (Volland, 1988). Another classification separates SSWsbased on their contortion of the polar vortex (Charlton and Polvani, 2007). A "vortex displacement" shifts the vortex off the pole, with the vortex forming "comma shape". A "vortex split" sees the vortex break up into two pieces of comparable size.

The impacts of SSWs can influence the polar atmosphere for months (see e.g. Baldwin and Dunkerton, 2001). For example, SSWs contribute to the size of the ozone hole via two different mechanisms. First, the warming of the stratosphere suppresses the formation of polar stratospheric clouds (Shen et al., 2020). These clouds are where ozone depleting reactions occur (Solomon, 1999) . Furthermore, the weakening of the vortex allows the intrusion of ozone rich mid-latitude air into the pole. Both these effects in combination lead to a smaller ozone hole (Solomon et al., 1986). The SSW also impacts the Southern and Northern Annular Modes (SAM and NAM). If easterlies appeared they can descend down into the troposphere, and push the SAM or NAM into a negative index for months (Shen et al., 2020; Taguchi and Hartmann, 2005).

The first observed Antarctic SSW

SSWs in the Southern Hemisphere are infrequent. The most notable occurred in September 2002. Here, 2002 (Allen et al., 2003) , when the vortex shifted off the pole and eventually spilt split into two. Later, one piece reformed into a weakened polar vortex (Ricaud et al., 2005). This impacted the ozone hole, which experienced 20% less ozone loss compared to previous years (Hoppel et al., 2003). An earlier SSW has been reported to have occurred in August-September 1988 (Schoeberl et al., 1989; Kanzawa and Kawa , While it is unclear if this even filled the The World Meteorological Organization (WMO) criteria for major or minor (Charlton and Polvani, 2007) SSW, Thompson et al. (2005); Kwon et al. (2020) have found this event to be one of the larger, early polar vortex weakening events.

In September 2019 a SSW occurred again. Within days, temperatures in the stratosphere increased by 50 K (Yamazaki et al., 2020). The vortex also shifted off the pole at higher altitudes, but remained centred over the pole, albeit with weaker winds, at lower altitudes, as we will show here. Whilst the 2002 SSW was classified as major, according to the WMO definition, the 2019 event was minor (Yamazaki et al., 2020). Due to their rarity, the causes of a SSW in the SH are not well understood. Eswaraiah et al. (2016, 2020a, b) have further reported of a less well known, a minor SH warming in September 2010. Whilst the 2019 and 2010 are both deemed minor, their dynamics were very different. The 2010 event had included a reversal of the temperature gradient poleward of 60°S from September 15, and the temperature increased by about 30 K at 80°S and 10 hPa (Eswaraiah et al., 2018). The zonal winds at 60°S at 10 hPa weakened by only 20-25 m/s (Eswaraiah et al., 2016). Henceit appears that the $ms^{-1}$ (Eswaraiah et al., 2016). Hence, the dynamical situation in 2010 dynamics were not very similar to was unlike those in 2002 and 2019, which both experienced rapid warming because in the latter two years, rapid warmings and wind reversals occurred. Instead of the WMO criteria, for example Kwon et al. (2020) have identified southern stratospheric polar vortex weakening events, showing that these happen more frequently than SSW events and with an increasing occurrence frequency since the 2000s.

It is widely accepted thought that SSWs are the product of an interaction between planetary waves and the atmospheric mean flow (Matsuno, 1971). The Arctic experiences more SSWs due to its geography. The North Pole is ringed by mountain ranges, perfect for producing atmospheric waves (Duck et al., 2001). An enhancement of wave activity over winter causes disruption

~~to the vortex, as the waves deposit their momentum at higher altitudes (Brasseur, 2005). However, Antarctica is enclosed by flat oceans, which don't excite waves as effectively as mountains (Holton, 2012).~~

NH has higher winter planetary wave activity and variability than the SH, thus leading to higher SSW occurrence in the NH. de la Cámara et al. (2019) have reported that about one third of sudden stratospheric deceleration events (events similar to SSWs) are preceded by anomalous wave activity from the troposphere. In two thirds of the events, the anomalous amplification of wave activity in the stratosphere that lead to the events, did not originate from the troposphere, but was likely linked to dynamics in the lower stratosphere and vortex geometry. As discussed by the recent comprehensive review of Baldwin et al. (2021, and references therein), the occurrence of SSW may be linked to various large scale oscillation modes in the atmosphere, including the Quasi-Biennial Oscillation (QBO, see e.g. Anstey and Shepherd (2014)), the Semiannual Oscillation (SAO), the El Ninõ-Southern Oscillation (ENSO, see e.g. Domeisen et al. (2019b)), ~~and~~ the Madden Julian Oscillation (MJO, see e.g. Wheeler and Hendon (2004); Schwartz and Garfinkel (2017))~~.~~, solar cycle, and extratropical blockings. Rao et al. (2019) also discuss these in detail, and provide an analysis of how each provided favourable conditions in the case of the NH 2019 SSW. Here, we will focus on ~~interactions between~~ the QBO and SAO in the SH context, and will not consider the ~~ENSO and MJO~~ others in detail.

The QBO is manifested in the reversal of zonal winds in the equatorial stratosphere. The ~~east~~ eastward and westward winds alternate every 22-34 months, with an average period of 28 months (Baldwin et al., 2001). This oscillation dominates the variability of the equatorial stratosphere, however, its influence stretches to both poles (Baldwin et al., 2001). The phases of the QBO have been found to influence the polar vortex and occurrence of NH SSWs. Holton and Tan (1980) were the first to propose that the QBO at 40-50 hPa modulates the subtropical zero wind line, which influences the propagation on waves in the stratosphere – a phenomenon known as the Holton-Tan effect (see Watson and Gray, 2014, and references therein). It was later discovered (concerning the NH) that the easterly QBO phase coincides with more SSWs (Richter et al., 2011). Other known nonlinear interactions with the QBO and SSW occurrence in the NH include those with the solar cycle (Labitzke, 2005) (for QBO at 45 hPa). Due to the scarcity of SH SSW events, similar relationships connecting the solar cycle, QBO and SSW occurrence have not been identified.

The Semiannual Oscillation is ~~a switching~~ an alternation of zonal winds in the equatorial mesosphere~~(Brasseur, 2005)~~. These winds swap between westerly and easterly, with a complete cycle taking six months. These wind shears descend down from above the mesopause into the upper stratosphere (Kawatani et al., 2020). The SAO amplitude has two peaks: one near the stratopause (1 hPa) and another close to the mesopause (0.01 hPa) (Kawatani et al., 2020). Westerlies near the stratopause maximise close to the equinoxes, whilst the easterlies maximise near the solstices~~(Brasseur, 2005)~~. The SAO maxima at 1 hPa exhibit a seasonal asymmetry, where the 'first cycle', which begins in December with the NH easterly phase, is stronger than the 'second cycle', which starts with the SH easterly, roughly in June (Garcia et al., 1997; Peña-Ortiz et al., 2010). This behaviour arises from differences in extra tropical wave forcing, which is generally understood to be stronger in the NH winter (Garcia et al., 1997). The drivers of the SAO are not well understood. The prevailing theories suggest that the westerly accelerations, in March and September, are caused by Kelvin and high frequency gravity waves~~(Brasseur, 2005)~~, whilst the easterlies maximise,

during December and June, from advection of easterly momentum across the Equator, by the upper branch of the Brewer-Dobson circulation (Smith et al., 2020).

Recent work by Gray et al. (2020) noted the importance of the equatorial mesosphere and upper stratosphere on forecasting Northern Hemisphere SSWs. Their modelling study ~~found~~ showed that SSWs were only reproduced ~~well~~ realistically when the flow in the equatorial upper stratosphere was constrained, simulating the two atmospheric modes in this region, the SAO and the QBO. Similar results were previously presented by Pascoe et al. (2006): In a troposphere-stratosphere-mesosphere global circulation model with forced QBO and SAO like variability, the timing of the NH mid winter warming advanced by about one month.

Whilst many studies have investigated the troposphere for answers to the questions raised by SSWs, we are ~~now beginning to see suggestions that we should also be looking at~~ here following suggestions that the upper atmosphere may be key to understand the drivers of SSWs. The works of Pascoe et al. (2006) and Gray et al. (2020) discussed above, ~~draws~~ draw attention to the upper atmosphere in the formation of a SSW, with a focus on the NH.

~~Here, we report on the interaction~~ In the present study, we analyze the behaviour of the QBO and SAO in the Southern Hemisphere during the winters of 2002 and 2019 ~~(the two years with SH SSWs)~~and two additional weak vortex event years, based on reanalysis data. ~~Both years exhibited clear easterly QBO conditions during the polar winter, leading to a comparison with other easterly QBO years in the SH. We find an interaction between the QBO and SAO during the austral winters of 2019 and 2002 that is unique in its timing and extent. Coinciding with the SAO-QBO interaction is an intensification of atmospheric wave propagation, which deposit easterly momentum in the upper atmosphere throughout the two winters, leading to a disturbed SH polar stratosphere and the observed SSW events.~~

## 2 Data and Methods

### 2.1 MERRA-2

The second Modern-Era Retrospective analysis for Research and Applications (MERRA Version 2, MERRA-2) is a National Aeronautics and Space Administration (NASA) atmospheric reanalysis product that begins in 1980 (Bosilovich et al., 2016). MERRA-2 has a horizontal resolution of $0.5° \times 0.625°$ with 42 ~~vertical levels~~ levels in the vertical from the surface to 0.01 hPa (Gelaro et al., 2017).

To investigate the connections between the SAO, QBO and SSW we used the four-times-daily zonal wind, geopotential height and temperature information of MERRA-2, averaged into daily means. We focus on the vertical pressure range of 550 to 0.1 hPa and the austral winter (~~June-July-August-September-October, JJASO).~~ June-September). Our analysis focuses mainly on the years 2019 and 2002, when SSW events took place in the Southern Hemisphere.

~~MERRA-2 was run in four production *Streams* (Bosilovich et al., 2016). The first three covered the periods 1980-1991 (stream 100), 1992-2000 (stream 200) and 2001-2010 (stream 300), and the final stream from 2011-present (stream 400). Each stream had initial conditions derived from MERRA with a subsequent single year spin-up period, details of the process can be found in Bosilovich et al. (2016); Bosilovich and Coauthors (2015); Gelaro et al. (2017).~~

In later analysis, were results from several years are averaged, the averaging is based on the streams. All years presented here were also analysed individually. The stream analysis ensures that decadal variability of the SAO and QBO interactions are not lost in a large average average, as the initial conditions change across the streams in MERRA2.

### 2.2 Semiannual Oscillation

Here, we focus our investigation on the easterly SAO maxima that occurs in the upper stratosphere, close to 1 hPa. The SAO is locked into the seasonal cycle (Kawatani et al., 2020), and is known to have a period of six months, but it has appreciable inter-annual variability (Smith et al., 2020). Here, we focus our investigation on the easterly SAO maximathat occurs close to Smith et al. (2017) report from multiyear satellite observations that the first easterly maxima, which occurs during the Northern Hemisphere winter has climatological equatorial zonal mean zonal winds between 20-30 m/s at 1hPa hPa, while the second maxima, occurring during the Southern Hemisphere winter., these peak between 0-20 m/s.

At 1 hPa MERRA-2 has been found to represent the easterly SAO in qualitative agreement with satellite derived winds (Kawatani et al., 2020), giving confidence that the SAO representation is reasonably realistic, particularly for the changes from westerly to easterly phases, and their propagation. . However, MERRA-2 has westerly bias compared to other reanalysis data and observations above 20 hPa. For the months considered here (June-September), Kawatani et al. (2020) show that the interannual variability in MERRA-2 SAO is comparable to other reanalysis data sets, suggesting that for our analysis, changes from year to year should be captured at a reasonable level.

For our analysis, will calculate the SAO equatorial wind amplitude at 1 hPa level by averaging over the equatorial latitudes 5°S–5°N from June to September. We will further estimate how far into the Southern Hemisphere the easterly wind pattern extends by finding the latitudinal location where the easterly winds turn westerly.

### 2.3 Quasi-biennial Oscillation

To analyse SAO and QBO interactions in the upper stratosphereHere, we focus on years with easterly QBO (eQBO) phase specifically in the equatorial upper stratosphere in the MERRA-2 zonal mean zonal wind . Analogous during June-July. Analogously to Rao et al. (2020c), we take the QBO phase at the 10 hPa pressure level, which Rao et al. Rao et al. (2020c) have shown to provide predictability in the SHSSW casesfavourable conditions for SSW occurrence the SH. QBO structure and dynamics in MERRA-2 reanalysis is are discussed in detail by Coy et al. (2016), who conclude that MERRA-2 displays a realistic QBO behaviourin zonal winds. We verified this by contrasting to sonde observations of zonal wind the zonal winds to radiosonde measurements from Singapore and found the two to be consistent, as expected (Coy et al., 2016).

For this study, eQBO is taken to be present if the mean June–July 10 hPa equatorial (5°S–5°N) zonal mean flow is easterlyduring the austral winter months of June/July. Both years 2019 and . The years fulfilling these conditions are 1980, 1983, 1985, 1988, 1990, 1993, 1995, 1997, 1999, 2002have an upper stratospheric eQBO present during the winter. This is not the case for the aforementioned year 2010, when the equatorial upper stratosphere exhibits a westerly QBO phase. , 2004, 2006, 2008, 2011, 2014, 2017, and 2019. We will discuss magnitudes of the eQBO winds during the eQBO years in the following sections.

To contrast the ~~two SSW years~~ SSW years of 2019 and 2002 to others with similar large scale equatorial flow conditions, other years with equivalent, i.e. eQBO phase, conditions during the austral winter months were analysed ~~. The~~ as a reference. Additionally, for the reference dataset, we leave out the early onset date (August onset) weak vortex years of 1988 and 2017 (Kwon et al., 2020). Thus, the 13 reference eQBO years in the MERRA-2 period ~~were~~ are 1980, 1983, ~~1988~~1985, 1990, 1993, 1995, 1997, 1999, 2004, 2006, 2008, 2011, ~~2014, and 2017. In later analysis, the easterly QBO years have been split by model stream: i.e. 1980, 1983, 1985~~ and ~~1990 are stream 100; 1993, 1995, 1997 and 1999 are stream 200; 2004, 2006 and 2008 are stream 300; and finally, 2011, 2014 are stream 400.~~ 2014.

~~We note that all years were analysed individually as well as in groups based on streams.~~

~~The~~ All years were initially analysed separately to check for conditions similar to year 2002 and 2019. As noted above, the years 1988 and 2017 ~~are left out of these groups as their dynamics were found to be unique, all experienced mesospheric wind reversals in October. These years were thus analysed individually, and will be discussed~~ were considered separately from the ~~other eQBO years.~~ reference data set, due to the early vortex weakening events. In 2017 the polar vortex has been reported to have experienced a disruption due to enhanced planetary wave activity throughout winter (Klekociuk et al., 2020). This lead to a smaller than average spring ozone hole (Klekociuk et al., 2020). There have also been reports of ~~an~~ a SSW occurrence in 1988 ~~(Kanzawa and Kawaguchi, 1990), but to our knowledge this has not been verified subsequently~~(Schoeberl et al., 1989; Kanzawa and Kawag , however, Thompson et al. (2005); Kwon et al. (2020) find this year to rather correspond to a weak vortex, wather than fulfilling SSW criteria.

### 2.4 Wave propagation

We ~~calculate the~~ use the quasi-geostrophic Eliassen-Palm flux (EP flux) ~~from MERRA2 fields~~ to visualise wave propagation and momentum ~~deposit. The EP flux is a vector in the meridional plane and its direction and magnitude portray the relative importance of the eddy heat fluxand the momentum flux (Brasseur, 2005). As planetary scale waves can only propagate where the zonal flow is westerly (eastward), the location of the zero-wind line (0 m/s) forms a barrier for planetary scale wave propagation.~~

~~The upward ($F_y$) and meridional ($F_\phi$) components of EP flux are :~~

$$F_y = f * a * d\theta/dp * \overline{u'v'}\cos(\theta)$$

$$F_\phi = -a * \overline{v'\theta'}\cos^2(\theta)$$

~~where $f$ is the Coriolis parameter, $d\theta/dp$ is the change of potential temperature $\theta$ with respect to pressure $p$~~deposition (as indicated by the divergence of the EP flux). ~~$u$ and $v$ are the zonal and meridional winds, respectively and $a$ is the radius of the Earth. Overbar denotes a mean and $'$ indicates deviation from the mean of the parameter in question~~Stationary and transient wave components are not separated, rather we analyse the total contribution from both.

~~The divergence of the EP flux indicates when and where momentum is being deposited. The~~ The convergence (negative values) and divergence (positive values) of the EP flux correspond ~~the~~ to deceleration and acceleration of zonal westerly winds

(Holton, 2012). The upcoming respectively. The EP flux results shown here were calculated from the MERRA-2 data fields: temperature, eastward wind, and northward wind ($T, u, v$), according to Edmon et al. (1980), with the additional scaling for display purposes as described by Bracegirdle (2011).

# 3 Results

## 2.1 Minor warming of 2019

Figures ?? and ?? show the different behaviour of Figure 1 presents the 7-day averages of zonal mean zonal wind ($ms^{-1}$), EP flux (arrows, $m^2s^{-2}$, reference arrow shown in the first panel) and EP flux divergence (grey contours, $\pm 2$ $ms^{-1}day^{-1}$ contours levels included) averaged for the reference years 1980, 1983, 1985, 1990, 1993, 1995, 1997, 1999, 2004, 2006, 2008, 2011, and 2014. The MERRA-2 zonal mean zonal wind reaches westerly velocities of over 100 $ms^{-1}$ in the polar vortex in the upper stratosphere (2 hPa , Figure ??) and the middle stratosphere (40around 1 hPa in June-July, after which the wind maximum descents down towards 10 hPa, Figure ??), as seen in the geopotential height of the two pressure levels. During the austral winter months, June to August, the polar vortex remains over Antarctica. However, following the onset of the SSW in September, the upper stratospheric vortex becomes offset from the pole, noted by the geopotential height minimum over the 120°W-40°E longitudinal sector, signifying a vortex displacement (Charlton and Polvani, 2007). At the same time, lower in the stratosphere, the minimum remains above Antarctica, as seen in Figure ??d. with peak velocities of 70 $ms^{-1}$ by mid-September. Consistent with the selection of eQBO years, we can see the easterly wind signature at 10 hPa at the equator, persisting throughout the time period and remaining well below the 1 hPa level. The easterly SAO wind pattern presents at around 1 hPa from June to early July, after which it subsides as the SAO annual cycle shifts to westerlies (Kawatani et al., 2020) . There is no clear merging of the eQBO and SAO wind structures. The figures also indicate the location where the zonal winds changes from easterly to westerly with a black solid contour (0 $ms^{-1}$, zero wind line). Propagation of stationary waves requires westerly flow, thus the zero wind line forms a barrier for stationary wave propagation.

The EP flux and its divergence indicate that from June to early-July the waves are generally acting to accelerate the zonal flow in the poleward side of the polar vortex and decelerating it on the equatorward side. This deceleration happens more consistently from mid-July onwards, at the same time as wave propagation upwards and equatorwards is enhanced above 100 hPa. The zero wind line at 10 hPa is initially located between 10°S-20°S, extending to 30°S from mid-August.

# 3 Results

## 3.1 SH polar winter 2019

Figure ?? 2 shows how the 7 day averaged zonal mean zonal wind (coloured, filled contours) evolves with time, along with the propagation of planetary scale waves during the austral winter of 2019, with the EP flux arrows illustrating the direction of wave movement. The Presentation and timing is analogous to Figure 1. As before, the location of the zero-wind zero wind line

(contour of ~~0 m/s~~ 0 $ms^{-1}$ zonal mean zonal wind~~velocity) , which forms a barrier for planetary wave propagation, )~~ is indicated as a thick ~~white line. Furthermore, the EP flux convergence (dashed line contour) indicates~~ black line. The EP flux divergence is shown with the grey dashed line indicating where the waves dissipate and deposit easterly momentum to atmospheric flow, acting to decelerate it ~~. The austral winterof 2019 saw the~~ at a rate of 2 $ms^{-1}day^{-1}$, and the grey solid line indicating where acceleration is taking place at a rate of 2 $ms^{-1}day^{-1}$.

Throughout the winter, the equatorial atmosphere around 10 hPa shows a easterly zonal mean zonal wind structure, with peak velocities of 30-40 $ms^{-1}$, indicating the presence of QBO in the easterly ~~descending phaseat 10 hPa (Figure **??**a). Note here that the~~ phase. This eQBO wind signal ~~already exists~~ is present around 10 hPa from early June, and is not initiated by the descending easterly SAO (seen here above 1 hPa), as may happen with wQBO (Kuai et al., 2009). ~~During late June the easterly phase of the SAO is present in the mesosphere (Figure**??**a). Poleward of the SAO signal, in the SH mesosphere, easterly momentum deposit is taking place, decelerating mesospheric flow. Later, between July 13-19 the SAO and QBO intersect south of the equator, forming a long zero wind line at roughly 30~~Contrasting to the reference (Figure 1), the equatorial SAO around 1 hPa is evident from mid-June, with zonal mean zonal winds of up to -20-30 $ms^{-1}$. The easterly wind structure extends further into the Southern Hemisphere (20°~~S that extends from 40 hPa to ~0.5 hPa (Figure **??**b). Easterly momentum continues to be deposited in the mesosphere, further decelerating the zonal wind. By August 24-30 the zero wind line formed by the QBO and SAO subsides and comes to sit between 40~~ S by late June) than in the reference, and ~~3 hPa (Figure **??**c). The zonal mean zonal wind in the mesosphere has decelerated from about 80 m/s to roughly 40 m/s, as a result of the continued momentum deposit. Furthermore, easterly momentum now continues to be deposited below and above the stratopause. Between September 7-13, when the SSW is observed in the stratosphere, zonal mean zonal wind in the mesosphere has reversed, with this easterly wind band connecting all the way through to the equatorial QBO (Figure **??**d). Easterly momentum continues to be deposited around the stratopause at high polar latitudes, moving further down into the stratosphere. Note that in this zonal mean picture the winds do not reverse down further than the mesosphere, but the winds in the stratosphere do weaken, from about 80 m/s to ~40 m/s. As will be discussed next, in this zonal average view with a longitudinal asymmetry as indicated by Figure **??**, the behaviour of the EP flux arrows~~ persists into mid-July, when it merges with the easterly wind structure that originates from the 10 hPa eQBO easterly wind structure.

From mid-June onwards, enhanced upwards wave propagation is taking place above 10 hPa and the wave convergence is driving enhanced deceleration on the equatorward side of the polar vortex. This can be seen clearly in Figure 3, which presents the 2019 anomaly relative to the ~~reversed zonal flow looks un-physical, i. e. it appears that wave propagation form the SH polar region towards the equator continues although the zonal mean zonal wind has turned easterly~~reference mean ("Figure 2" - "Figure 1"). Unlike in late-August, when enhanced upwards wave flux originating from the troposphere (Eswaraiah et al., 2020a; Shen et al. is taking place across the stratosphere, the earlier enhanced upwards flux is limited to 10 hPa and above.

~~When Figure **??**d is averaged in accordance to how the vortex shifted, as seen in Figure **??**, clockwise from~~ Initially in early June, enhanced easterly momentum deposition is taking place between 40°~~E to 140~~S-60°~~W and from 140~~S, decelerating the flow above 1 hPa. This extends downwards and equatorwards, resulting in consistent deceleration of the upper stratospheric flow between 20°~~W to 40~~S-50°~~E, respectively, we find more consistent behaviour in the mesosphere and upper stratosphere.~~

~~This is shown in Figure ??a, where the mesospheric and upper stratospheric winds (down to about 20 hPa) at~~ S from mid-June throughout July. At the same time the zonal wind is accelerated by 10-20 $ms^{-1}$ around 60°S~~reverse on the mainly Eastern side of Antarctica, connecting into the equatorial QBO. On the largely Western side on the Antarctica, in the sector encompassing the shifted vortex ,~~. This leads to a more vertically aligned structure of the ~~westerlies shift towards South America, and reverse over the pole as seen~~ polar vortex zonal mean zonal wind, rather than the typical structure, which we can see in Figure ~~??b, providing a pathway for wave propagation towards the equator .~~ 1, tilted towards equator in the upper stratosphere. This appears to correspond a vortex shape Albers and Birner (2014) found typical for NH split type SSW events.

~~An alternate view of the coupling of the SAO and QBO wind signals averaged over the latitudinal range of 15~~From late-June the direction of wave propagation in the upper stratosphere is guided by the easterly wind structure near 1 hPa. By early-July the convergence of the EP flux contributes to deceleration of the stratospheric flow above 10 hPa around 20°~~S-20°Sis shown in Figure ??, which presents how the daily zonal mean zonal winds from 100-0.1 hPa evolve over June and July. The SAO is visible in the mesosphere in June and we can see the SAO pattern descending, before the it connects to the eQBO wind pattern in July~~S, leading to a structure that resembles merging of the previously separate easterly wind structures of the SAO and eQBO. The formed zero wind line guides more wave upwards. Through out July and into August the zonal mean zonal wind is consistently weaker by 10-20 $ms^{-1}$ across the stratosphere between latitudes of 60°S and 40°S. By late-August, when we observe enhanced upwards wave propagation from the troposphere, the zonal flow is further rapidly decelerated above 10 hPa, leading to the SSW conditions in September.

### 3.2 ~~Major warming of 2002~~

~~Figure ?? is analogous to Figure ??~~

### 3.2 SH polar winter 2002

Figures 4 and 5 are analogous to Figures 2 and 3 but now for the austral winter of 2002. Again ~~the QBO is easterly~~ we observed the eQBO wind structure at 10 hPa from early June, similar to 2019. ~~Between June 8-14 an~~ From June 8 onwards, the easterly oscillation of the SAO is present ~~in the mesosphere as seen in Figure ??a. Easterly momentum is also deposited throughout the mesosphere and upper stratosphere at roughly~~ around 1 hPa and upwards wave propagation is enhanced throughout the stratosphere above 100 hPa. Between about 40°S and 60°S ~~, leading~~ enhanced easterly momentum deposition throughout the atmosphere above 10 hPa, lead to deceleration of the zonal winds in this region throughout the time period. ~~In Figure ??b (June 15-21) the~~ As in the case of the winter of 2019, we see a merging of the previously separate easterly wind structures of the SAO and eQBO~~wind patterns intersect, similar to~~ . This now takes place mid-June, approximately four weeks earlier than in 2019. The zero wind line of the zonal mean zonal wind, formed as a result, extends to 30°S, cutting across ~0.4–30 hPa.

This vertical extend is not maintained for extended periods of time. However, as in 2019, ~~well before the SSW event. The resulting~~ the latitudinal location of the zero wind line ~~extends from roughly 30 hPa to 0.3 hPa close to~~ between 1–50 hPa is shifted about 10 degrees polewards from its typical location (Figure 1) throughout July, to about 30°S~~, extending the barrier for~~

planetary wave propagation into the SH mesosphere and upper stratosphere. During this time easterly momentum continues to be deposited in the mesosphere.

After this intersection, eQBO comes to lay between 50-2 hPa extending to about In both cases, the merging of the two initially separate easterly wind patterns, the resulting shift in the zero wind line across the month of July, well before the SSW onsets took place in September, and the enhanced zonal flow deceleration above 10 hPa appear notable.

Overall, the atmospheric response above 10 hPa is remarkably similar to 2019: Both years show sustained wave driven deceleration of zonal mean wind between 40°S from S-60°S from June, throughout July, and simultaneous acceleration between about 60°S-70°S. By early to mid-August the zonal winds have decelerated across the polar region above 1 hPa.

Identical analysis for the previously identified early weak vortex event years of 1988 and 2017 show that a similar equatorial easterly wind pattern mergers took place during both winters (figures included as supplement). In 2017 this happened in late June, accompanied by enhanced upwards EP flux, and followed by a poleward shift in the equator (Figure ??c), pushing the zero wind line with it and thus blocking wave propagation towards the equator throughout most of the upper stratosphere. Easterly momentum continues to be deposited in the mesosphere and upper stratosphere. By this time the winds throughout the polar atmosphere have decelerated, latitudinal location. In 1988 this happened much later, from 20 July onwards. In 1988, however, there is no indication of enhanced upwards wave propagation in the lead up to the SSW . In Figure ??d, we see the polar winds dramatically reverse between September 21-27 from 0.1 hPa down to about 50 hPa, coinciding with the June, as was the case for 2002stratospheric warming, 2017, and 2019.

### 3.3 Weak vortex events in context of other eQBO years

When analysing all the eQBO years individually the type of equatorial wind pattern merger reported above either did not take place, or took place much later, and, like in 1988 was not accompanied by enhanced upwards wave flux.

Based on these results it appears that for the SSW cases and the weak vortex cases, there is an interplay of early winter wave forcing and the wave guide formed by the zonal mean zonal wind structures to do with the equatorial easterly winds related to the SAO around 1 hPa and the equatorial easterly winds related to the QBO around 10 hPa. We will now proceed to investigate if these factors together provide predictability for the weak vortex events.

The time top left panel in Figure 6 presents the temporal evolution of the zonal mean winds at 157-day mean magnitude of the equatorial zonal mean zonal wind averaged over 5°S-20S-5°S during June-July N for the 1 hPa level, representing the upper stratospheric SAO. The years 1988, 2002is shown in Figure ??. Here we see the eQBO and easterly SAO wind patterns interacting somewhat earlier that for , 2017, and 2019 (Figure ??), now starting in the first half of June. have been labeled separately, while all other eQBO years are shown as grey lines. Years 2002, 2017, and 2019 have some of the highest easterly wind velocities reaching 10 $ms^{-1}$ and higher in June. In this context we should note again that the results of Kawatani et al. (2020) suggest that interannual variability in MERRA-2 is consistent with other reanalysis datasets, but that MERRA-2 has a westerly bias above 20 hPa. The year when the June velocities reach $-30$ $ms^{-1}$ corresponds to the first MERRA-2 year, 1980.

### 3.4 ~~Comparison to other eQBO years~~

~~With the indication that the SAO and the eQBO winds interacted in the months leading up to the SSW events in~~ The bottom left panel presents a similar zonal wind temporal evolution (averaged over 5°S-5°N), but now for the QBO level of 10 hPa. Again, the years 2002, 2017, and 2019 ~~, we now proceed to investigate other potential occurrences of this type of coupling during SH winter months.~~ show some of the largest easterly velocities, between $-20$– $-40$ ms$^{-1}$ in June-July. While the SAO is known to occur regularly, but with appreciable inter-annual variability (Smith et al., 2020)~~. The~~ , as we seen in Figure 6, the QBO on the other hand has an average period of 28 months.

#### 3.3.1 ~~SAO-QBO interaction in 1988 and 2017~~

We can see this in the temporal evolution of the equatorial 10 hPa winds: in some cases the winds remain westerly for much of June before shift to the easterly phase, while in 1988, the phase changes from easterly to westerly in July.

~~In our analysis of individual years we found wave-mean flow interactions similar to the cases of~~ The panels on the right hand side of Figure 6 show the mean and median latitudinal locations of the zero wind line (zero $U$) at 1 hPa (top) and 10 hPa (bottom). The grey error bars indicate one standard deviation ($1 \times \sigma$) around the mean latitudinal location. As before the years 1988, 2002, 2017, and 2019 ~~and 2002 taking place on two additional austral winters: 1988 and 2017.~~ have been labeled separately.

~~The winter of 1988 has a close resemblance to 2019, but the SAO-QBO interaction occurs about a week later, with similar, sectoral wind reversal patterns to 2019 delayed to late September in 1988. Figure 9 is as Figure **??**, but for the austral winter of 2017. Figure9a shows the easterly SAO in the mesosphere and the QBO in the stratosphere. Poleward of the SAO in the mesosphere, EP flux convergence similar to~~ At 1 hPa, the years 2002, 2017, and 2019 ~~is taking place. The SAO and QBO features intersect earlier, between June 29 - July 5, creating an extended zero wind line at 30~~all show significant (beyond $2 \times \sigma$) southward shift of the location where winds turn from westerly to easterly in the meridional direction. While the mean location remains close to the equator, for 2002, 2017, and 2019 we see a shifts to locations between 15°~~S from 40 hPa to 0.3 hPa , Figure 9b. As before, the zero wind line subsides in August, Figure 9c, extending now from 40 hPato 3 hPa. Meanwhile, easterly momentum continues to be deposited in the mesosphere throughout these winter months, but this is does not extend as far into the stratosphere as in 2002 and 2019. This likely leads to delays in the wind reversal, which now takes place during October 23-29, Figure 9d.~~

#### 3.3.1 ~~Remaining eQBO years~~

~~Here, we present similar analysis to Figures **??** and **??**, however, instead of individual years, the averaging is now based on the MERRA-2 streams (Bosilovich et al., 2016) described in section 2.1. Note that all years were initially analysed individually – the stream averages were found to be representative of the individual years, and no SSW like behaviour was observed for the individual years.~~

Figure ?? shows the zonal wind, EP flux and EP flux convergence averaged over June15-21, July 6-12, August 10-16 and August 31 - September 6, averaged for the years 1980, 1983S and about 27°S. This takes place in June, 1985 and 1990. In Figures ??a and b, the SAO wind pattern is noticeable, but not as distinct as before, above while for 1988, the shift is seen later at a time when there is in general more variability as shown by the large $1 \times \sigma$ bar.

At 10 hPa there is not as clear of a shift as we see at 1hPa. Figures ??c and d, show how the easterly QBO evolves, but no noticeable easterly momentum is deposited. No SAO-QBO interaction is taking place during hPa. However, in all cases the latitudinal location where the 10 hPa winds change direction is preferably in the SH poleward range, between 18°S and 30°S in June-July. For 1980 and 1983 we find the SAO-QBO interaction taking place, but much later in winter, late July/early August, compared to 2002 and 2019, and the This could suggest that the SSW events in the SH are sensitive to the timing of the eQBO phase during the polar winter.

Considering the shift in the location of the zero wind line in both cases does not extend into the mesosphere, leaving the wave propagation pathway to the equator accessible.

Figure ?? is the same as Figure ?? but now averaged for the years 1993, 1995, 1997 and 1999. The results are very similar to at 1 hPa, we now examine if this could be used with a measure of the wave forcing to identify SH SSW/weak vortex events. Figure ??; Figures ??a and bshow the SAO in the mesosphere in June and July. Figures ??c and d show the enlargement of the eQBO wind pattern and the return of westerlies to the Northern Hemisphere. None of the individual years displayed a SAO-QBO interaction similar (with regards to timing and zero wind line extent) to 2002 and 2019 at any point during winter. Figure ?? is the same analysis but 7a) shows the upper stratospheric EP flux divergence on the equator side of the polar vortex edge (see Figure 1), averaged between 1-10 hPa and between latitudes 50°S-40°S (in units of $ms^{-1}day^{-1}$) versus the average latitude of the zero wind line at 1 hPa. Both variables are averaged from mid-June to mid-July, identified as a potential key timing from Figure 6. In Figure 7b) the averaging period is shifted by 14 days to 29 June–26 July. For each of the following panels the zero wind line averaging time periods remain the same in the respective columns, while the averaging period of the EP flux divergence changes, as given in the panel title. Panels c) to f) correspond to the lower stratospheric EP flux divergence, again on the equator side of the polar vortex edge, now averaged for the years 2004, 2006 and 2008. Figure??anow shows the SAO in the mesosphere in June, similar to 50-70 hPa and 60°S-40°S.

In mid-June to mid-July in the upper stratosphere (Figure 7a) in mid-June to mid-July the zero wind line is located north of the equator, but has moved clearly southward in 2002 and 2019. The SAO and QBO show signs of early interaction, but, this is not sustained 2019, with EP flux divergence between $-3$ to $-2.5$ $ms^{-1}day^{-1}$. We also see a large southward shift of over 10° in 1980, 1990, and 2017, but these years no not exhibit similar zonal flow deceleration from wave forcing. As discussed earlier, the year 1980 had the largest amplitude of the SAO zonal wind (Figure ??b)in late July. This results in a zero wind line between roughly 6), and upon further investigation, the year 1990 is also amongst the large June amplitude SAO wind years, with peak wind easterly velocities of 10-15 $ms^{-1}$. Both however, have a changing 10and 1 hPa , smaller vertical extent than the two in hPa QBO phase in June, unlike 2002and 2019. Figures ??c and d show eQBO enhancement and the return of westerlies to the NH as austral winterfades into spring.

The average for the remaining eQBO years, 2011 and 2014, is shown in Figure **??**. In early July (much later than the other years analysed) we find a weak SAO signal at 1 hPa (Figure**??**a) , and it does not extend further into the SH as happened in 2017 and 2019 and 2002. Thus no early winter momentum deposit takes place in the winter mesosphere. The SAO and QBO intersect (Figure**??**b)in late July, triggering easterly momentum deposit in the polar mesosphere. However, much like in Figure **??**, this SAO-QBO pattern is not pushed beyond 30°S, unlike during the SSW years. The QBO stays enhanced into August (Figure **??**c). The QBO eventually subsides into the lower stratosphere in September, Figure **??**d. which show eQBO from start of June. This suggest that the SAO amplitude alone is not sufficient to understand later vortex weakening events, but should be viewed in context of the QBO phase in early winter.

In general, the QBO and SAO both appear in the years analysed here, however, their vertical and poleward extents vary. This seems to influence the timing and extent on the SAO-QBO interaction. The two SSW years Shifting the time period later (Figure 7b), now shows a similar response for the year 2017, with an average zonal flow deceleration of over 4 $ms^{-1}day^{-1}$ along with a shift in the zero wind line latitude to south of 20°S.

In the lower stratosphere the early winter period (Figure 7c) now clearly separates the weak vortex years of 2002, 2017, and 2019 by southward shift of the zero wind line location accompanied by EP flux convergence. In the later time period (Figure 7d), we find the years overall much more scattered, with no clear distinction of the weak vortex events.

Finally, we examined if the early winter zero wind line at 1 hPa could be used to identify the SSW years based on the August–September EP flux divergence in the lower stratosphere. Figures 7e)-f) show the EP flux divergence averaged for the time period of 10 August–6 September, while the zero wind line time period remains consistent with the previous panels. We can now see that the years 2002 and 2019 , have a large (vertical and poleward extent) eQBO at 10hPa, and alarge (vertical and poleward extent)SAO in the mesosphere before their intersection in July, which produces a have a very close resemblance to the early winter in the upper stratosphere (Figure 7a), being clearly separated from the other years both in the zero wind line stretching from the stratosphere into the mesosphere. The SSW-like years of 1988 and location and the wave momentum deposition. This is not the case for the weak vortex year of 2017have similar early winter behaviour to 2002 and 2019, however, mesospheric wind reversal takes place later. The 1980s and 1990s were characterised by having both a smaller QBO and SAO which only occasionally interacted in late winter. Whilst the 2000s had a smaller QBO and larger SAO, which interacted but did not produce a , however. Kwon et al. (2020) report the 2017 vortex weakening onset date as August 22. We proceeded to test delayed time periods for the EP flux divergence, but these did not indicate change beyond the roughly $-1$ $ms^{-1}day^{-1}$ range for the year 2017.

We also tested the used of the 10 hPa zero wind line similar to the SSW years. The 2010s had a large eQBO , with a smaller SAO which did interact in July, however, no SSW was produced in September. This suggests that not only may the particular phases be important for preconditioning the area for a SSW, but there vertical and poleward extents (and thus any mechanisms influencing these)seem to also be a factorlocation to see if a measure of the eQBO wind pattern horizontal extent would provide similar results (not shown). As could be expected from Figure 6, this was unsuccessful and the years were simply separated by the difference in EP flux divergence (identical to Figure 7 separation on the y-axis).

While the EP flux convergence, particularly in the upper stratosphere, in early winter would on its own provide some predictability for later conditions, the zero wind line location at 1 hPa appears to add additional separation, particularly when used for the lower stratospheric EP flux divergence (Figure 7c).

## 4 Discussion

The sudden stratospheric warmings over Antarctica in 2002 and 2019 both have an early winter equatorial ~~SAO-QBO~~ SAO-QBO-like wind pattern interaction and coinciding easterly momentum ~~deposits~~ deposition in the polar ~~mesosphere~~atmosphere, as indicated by the EP flux convergence. For both years the SAO is ~~a clear~~ presents as a feature of easterly winds (of over 10 $ms^{-1}$) extending into the SH ~~before it reaches 1 hPa. This shift from (polar) westerly to (low latitude) easterly winds changes~~ from early winter. Change in the latitudinal location where winds shift from westerly to easterly influences the waveguide in the ~~mesosphere, which results~~ upper stratosphere-lower mesosphere, resulting in easterly momentum being deposited ~~in the mesosphere~~ on the equatorward side of the polar vortex from early winter. When the QBO and SAO easterly wind features merge, they generate a zero wind line that stretches from the lower stratosphere into the mesosphere (~30 hPa to 0.3 hPa) near 30°S latitude, now modulating the wave guide across the whole vertical range. This ~~QBO feature then continues extending~~ feature continues to be extended towards the pole into August, with continued easterly momentum ~~deposit~~ deposition in the polar ~~mesosphere~~atmosphere, decelerating the ~~mesospheric westerlies . By September, the extended momentum deposit results in reversal of mesospheric winds. The year~~ prevailing westerlies on the equatorward side of the polar vortex. In 2002~~saw~~, the zonal mean zonal winds between about 40°S-60°S decelerate down to below 10~~hPa. However~~ hPa, eventually triggering major SSW conditions. In contrast, in 2019, the ~~mesospheric~~ zonal mean zonal wind reversal ~~links across latitudes from the pole to the equatorial QBO~~is less focused, taking place across a wider range of latitudes, and major SSW conditions are not fulfilled. In our zonal mean analysis, this suggests that vertical wave propagation from the source regions at high and mid-latitudes is significantly affected, with the movement of the zero wind line creating a barrier for ~~upwards~~ wave propagation.

~~The SSW-like~~ We found that the weak vortex years of 1988 and 2017 show a similar SAO-QBO ~~interaction~~ wind pattern like merging in July. ~~Whilst the winds did reverse in the mesosphere in late September-October (later than we found for 2019 and~~ However, neither of these years show a poleward shift in the zero wind line location as early as was seen for 2002 ~~), there does not appear to be a rapid warming similar to 2019~~ and ~~2002. Although,~~ 2019. Causes of these differences could be investigated further in a detailed study. We note that in 2017, the changes in dynamics were enough to stifle the growth of the ozone hole (Klekociuk et al., 2020). ~~Causes of these differences should be investigated further in a detailed study of these SSW-like years.~~

Our analysis of all other years with similar background QBO conditions in MERRA-2 did not reveal similar behaviour with early winter ~~momentum deposit and similar SAO-QBO interaction. Hence we proceeded to further analyse the other eQBO years by decades of matching MERRA-2 streams. The general behaviour of the polar atmosphere during eQBO in the 1980s and 1990s was similar. In general, both decades show a weak signature of the SAO in the mesosphere. However, the SAO-QBO interactions were either: later in the season (August) or did not result in a clear poleward shift of the zero wind line. We did~~

not find evidence of easterly momentum being deposited throughout the winter as we did for 2002 or 2019. The later decades, the 2000s and 2010s, did in general have a SAO present in the mesosphere in early winterand the SAO and QBO did interact in July, similar to 2019. However, this did not result in continued deposition of easterly momentum through the winter, or mesospheric wind reversals in September. sustained momentum deposition and similar merging of SAO-QBO-like easterly wind patterns in early winter.

Recently, Gray et al. (2020) reported that in order to accurately simulate predict NH SSWs in an atmospheric model, not only was is it was necessary to constrain the model's global tropospheric winds and temperatures, but further constraining of and to further constrain the zonal wind in the equatorial atmosphere above 5 hPa to reanalysis fieldswas also needed. These model results further emphasize those of Gray (2003) who showed similar results for a middle atmosphere only model: that the high altitude equatorial atmosphere plays an important role in NH extreme eventsSSWs. Although our analysis focuses on the SH SSWs in 2002 and 2019, our results present a possible physical mechanism for this connection. The early winter equatorial SAO-QBO interaction wind pattern interaction with the simultaneous EP flux convergence, and subsequent modulation of the wave guide waveguide, reflects mid-latitude waves up and pole-ward, resulting in easterly momentum deposit in the mesosphere. The SAO-QBO interaction is deceleration of the equatorward side of the polar vortex above 100 hPa. The SAO-QBO-like interaction was not unique to 2019 and 2002 and was found to happen during other easterly QBO years. However , apart from the two SSW-like years of 1988 and 2017, the the early timing and extent of the zero wind line was not found to polerward shift did not occur in these other years. We Our results suggest that this may be a reflection of variations not only in QBO, but also in the amplitude and descent pattern of the SAO, the latter of which, to our knowledge, are not well understood (see e.g. Moss et al., 2016; Kawatani et al., 2020). While we focused particularly in scarce SH SSW/weak vortex events here, the the seasonal evolution of the SH polar vortex and predictability of related climate patterns has been investigated for example by Lim et al. (2018) and Byrne and Shepherd (2018).

We propose that this early winter behaviour may be a key physical process in decelerating the mesospheric aid in identifying conditions that lead to deceleration of the polar winds, which may could then precondition the atmosphere for a SSW. For example in 2019, when there was enhanced upwards wave flux in August (Shen et al., 2020), the modulated waveguide in the stratosphere and above may have provided further optimal conditions for large disturbance to take place. It may also help partially explain why SSWs are less common in the Southern Hemisphere: if the early and large SAO-QBO interaction is dependent on both SAO-QBO-like merging contributes to optimal conditions for SSW, not only is this dependent the QBO being in the correct phase, and the SAO appears to need to have but also the SAO having a large amplitude and descend down into the stratosphere during the early-mid winter. The SH winter typically experiences smaller amplitude SAO easterlies, while the NH winter experiences much larger easterly winds (Smith et al., 2017). However, this hypothesis would need to be tested separately for the NH. It is also important to note again that the NH has higher winter planetary wave activity and variability than the SH.

As we find that the early key these early patterns start occurring 2-3 months before the SSW eventor vortex weakening events, the behaviour of the equatorial middle atmosphere along with the polar response at this stage may heed signal an imminent SSW event, potentially providing predictability beyond the current 20-30 typical 10-15 day window in SSW prediction on

both hemispheres (Lawrence and Manney, 2020; Rao et al., 2020c). This in turn in the NH (Domeisen et al., 2020), with some signals possibly appearing as early as 30 days in advance (Lawrence and Manney, 2020). As reported by Rao et al. (2020c), for the 2019 SH minor SSW, the predictive limit from forecast models was 18 days. The results reported here could potentially aid subseasonal to seasonal (S2S) prediction (Domeisen et al., 2019a)(Domeisen et al., 2019a, 2020). However, this would as the motivation for this study was to better understand early signals for the 2019 SH event, this will need to be tested in detail for the NH atmosphere first. We note that the results presented by Gray et al. (2020) (their Figures 3-4) suggest that coupling of the SAO and QBO zonal wind patterns, similar to our SH cases, took place in their simulation approximately 2 months before the onset of the NH January 2009 SSW. As noted by Gray et al. (2020), the atmospheric region where the SAO originates (mesosphere), tends to be neglected in model development. Our results provide further evidence that these mesospheric altitudes are not only important for understanding the NH but also the SH extreme dynamical events. As noted by the multi-model study of Rao et al. (2020b), representation of the QBO is also remains a challenge.

As mentioned earlier, much work has been done in understanding both causes and implications of SSWs, particularly in the NH. Baldwin et al. (2021) provide a recent review of the current understanding, including the many Many interactions with large scale atmospheric modes that or external forcing have been found to influence NH SSW occurrence, including the QBO, the ENSO, solar cycle, and the MJO. Due to the scarcity of SH SSW events we were unable to investigate the potential individual influences of these. However, we note that ENSO conditions, based on the Multivariate ENSO Index (MEI.v2, Zhang et al. (2019) available at , last accessed 3 Dec, 2020Zhang et al. (2019); Multivariate ENSO Index Version 2 (MEI.v2)), were neutral, while the MJO index (Wheeler and Hendon (2004), available at , last accessed 3 Dec, 2020) amplitude (Wheeler and Hendon, was positive, during both 2002 and 2019. Note that the MJO index amplitude corresponds to $\sqrt{\text{RMM1}^2 + \text{RMM2}^2}$, as defined by Wheeler and Hendon (2004), and does not account for the MJO phase. For the SSW-like weak vortex years of 1988 and 2017 the MJO was generally variable during the austral winter, while the ENSO index was negative, and thus opposite to the two generally recognised SSW years. These difference differences could signal the importance of teleconnections in the SH polar responses.

## 5 Conclusions

Sudden stratospheric warmings are disruptions to the seasonal cycle of the polar winds. Only two well-documented ones have occurred over Antarctica: one a major SSW in 2002 and another in 2019. a minor one in 2019, although Kwon et al. (2020) have noted an increasing trend in the number of southern stratospheric polar vortex weakening events in the last two decades. Here we present results based on the MERRA-2 reanalysis, showing that during both years, 2002 and 2019:

1. From early winter, waves are depositing momentum in the polar mesosphere equatorward side of the upper-stratospheric–lower mesospheric polar vortex in a manner that is consistent with the equatorial SAO pushing the wave guide upper stratospheric SAO-like wind structure pushing the waveguide boundary into the SH . extratropics.

2. ~~An early winterSAO and QBO interact~~ In early winter, SAO and QBO-like wind patterns merge in the equatorial atmosphere, driving further momentum ~~deposit~~deposition, and thus zonal wind deceleration, in the polar ~~mesosphere.~~ vortex.

3. Changing zonal ~~winds further influencing~~ wind further influences wave propagation conditions, ultimately transferring the signal to the ~~stratosphere and triggering SSW conditions~~ lower stratosphere, likely contributing to favourable propagation conditions for enhanced tropospheric wave forcing later in the winter, resulting in the observed SSWs.

~~For both years the SAO is pronounced before it reaches 1 hPa, and easterly momentum is deposited in the mesosphere before the intersection, and is sustained throughout the season. When the equatorial eQBO and SAO wind patterns interact they result in a zero wind line that stretches from~~ Years 2002, 2019, and the ~~lower stratosphere into the mesosphere near 30°S, modulating the wave guide~~early onset vortex weakening event year of 2017, all depict some of the highest easterly equatorial upper stratospheric SAO zonal mean zonal winds ($U_{1\text{hPa}} < -10$ ms$^{-1}$) in June. These are accompanied by a significant ($> 2 \times \sigma$) southward shift of the latitudinal location where zonal winds reverse direction from (polar) westerly to (equatorial) easterly. Along with the high amplitude SAO winds, these years also show easterly 10 hPa QBO throughout June ($-35$ ms$^{-1} < U_{10\text{hPa}} < -20$ ms$^{-1}$), suggesting that the SAO amplitude alone is not sufficient to understand these SH vortex weakening events, but the QBO phase in early winter also plays a role.

Previous work focused on the more frequent NH SSWs has pointed to the role of the equatorial upper stratosphere and mesosphere particularly when ~~simulating~~ predicting the timings of NH SSW (Gray et al., 2020). Our analysis of the two SH SSWs suggest that, at least for the Southern Hemisphere, the ~~interaction of the QBO and the SAO~~ merging of the eQBO and the SAO-like wind patterns in the equatorial upper stratosphere-mesosphere seems critical in triggering the polar disturbances. The ~~SAO-QBO interactions~~ wind pattern in 2002 and 2019 ~~are~~ is not unique, however, ~~the coupling and extent of the equatorial wind patterns occur~~ this occurs much earlier in the season ~~and result in a longer~~ than other easterly QBO years, leading to early winter deposition of momentum, as indicated by the EP flux divergence, that decelerates the winds in the equatorward side of the polar vortex by $-3$ to $-2.5$ ms$^{-1}$day$^{-1}$ from mid-June onwards.

When considering the early winter EP flux divergence together with the latitudinal location of the zero wind line ~~when compared to most other easterly QBO years . We propose~~ at 1 hPa, we were able to identify the SSW/early onset vortex weakening event years up to 60 days before the events. We postulate that this early winter behaviour may be a key physical process in decelerating the ~~mesospheric~~ polar vortex winds, leading to preconditioning of the polar atmosphere for a SSW. The occurrence of these patterns in the equatorial atmosphere and in the polar ~~mesosphere~~ upper atmosphere during early winter could provide extended predictability of SSWs from the ~~current 20-30 day window (Lawrence and Manney, 2020; Rao et al., 2020c) to 2-3 months.~~ typical 10-18 day window (Domeisen et al., 2020; Lawrence and Manney, 2020; Rao et al., 2020c).

As our present analysis is ~~based on SSWs~~ focused on events that took place in the SH, further work would be needed to test to what extent ~~SAO-QBO interactions~~ these SAO-QBO-like patterns might play a role in NH SSWs. This future work may help shed light on the different roles background flow and wave enhancement have on triggering the SH and NH SSWs, which may help explain why SH SSWs occur less frequently than NH SSWs.

*Data availability.* The MERRA-2 dataset is freely available (see Global Modeling and Assimilation Office (GMAO), 2015). The ENSO Index, MEI.v2 (Zhang et al., 2019) is freely available (see Multivariate ENSO Index Version 2 (MEI.v2)). The MJO index (Wheeler and Hendon, 2004) is freely available (see Madden–Julian oscillation index (MJO)).

*Author contributions.* AS and VJN planned the study, analysed the MERRA-2 data and contributed to the writing of the article.

*Competing interests.* The authors declare no competing interests.

*Acknowledgements.* We are grateful for the open access to the MERRA-2 reanalysis data products provided by GES DISC. The work of VJN was supported by a postgraduate scholarship provided by the University of Otago Physics Department.

## References


Albers, J. R. and Birner, T.: Vortex Preconditioning due to Planetary and Gravity Waves prior to Sudden Stratospheric Warmings, Journal of the Atmospheric Sciences, 71, 4028–4054, https://doi.org/10.1175/jas-d-14-0026.1, 2014.

Allen, D. R., Bevilacqua, R. M., Nedoluha, G. E., Randall, C. E., and Manney, G. L.: Unusual stratospheric transport and mixing during the 2002 Antarctic winter, Geophysical Research Letters, 30, 1599, https://doi.org/10.1029/2003GL017117, 2003.

Anstey, J. A. and Shepherd, T. G.: High-latitude influence of the quasi-biennial oscillation, Quarterly Journal of the Royal Meteorological Society, 140, 1–21, https://doi.org/10.1002/qj.2132, 2014.

Baldwin, M. P. and Dunkerton, T. J.: Stratospheric Harbingers of Anomalous Weather Regimes, Science, 294, 581–584, https://doi.org/10.1126/science.1063315, 2001.

Baldwin, M. P., Gray, L. J., Dunkerton, T. J., Hamilton, K., Haynes, P. H., Randel, W. J., Holton, J. R., Alexander, M. J., Hirota, I., Horinouchi, T., Jones, D. B. A., Kinnersley, J. S., Marquardt, C., Sato, K., and Takahashi, M.: The quasi-biennial oscillation, Rev. Geophys., 39, 179 – 229, https://doi.org/10.1029/1999RG000073, 2001.

Baldwin, M. P., Ayarzagüena, B., Birner, T., Butchart, N., Butler, A. H., Charlton-Perez, A. J., Domeisen, D. I. V., Garfinkel, C. I., Garny, H., Gerber, E. P., Hegglin, M. I., Langematz, U., and Pedatella, N. M.: Sudden Stratospheric Warmings, Reviews of Geophysics, 59, e2020RG000 708, https://doi.org/10.1029/2020RG000708, 2021.

Bosilovich, M. G. and Coauthors: MERRA-2: Initial Evaluation of the Climate, Technical Report NASA/TM–2015-104606/Vol. 43, National Aeronautics and Space Administration, Goddard Space Flight Center, Greenbelt, Maryland 20771, https://gmao.gsfc.nasa.gov/pubs/docs/Bosilovich803.pdf, Technical Report Series on Global Modeling and Data Assimilation, Volume 43. Last accessed 24 Nov, 2020., 2015.

Bosilovich, M. G., Lucchesi, R., and Suarez, M.: 2016: MERRA-2: File Specification. GMAO Office Note No. 9 (Version 1.1), Tech. rep., Global Modeling and Assimilation Office Earth Sciences Division NASA Goddard Space Flight Center, Greenbelt, Maryland 20771, http://gmao.gsfc.nasa.gov/pubs/office_notes., last accessed 24 Nov, 2020, 2016.

Bracegirdle, T. J.: The seasonal cycle of stratosphere-troposphere coupling at southern high latitudes associated with the semi-annual oscillation in sea-level pressure, Clim. Dyn., 37, 2323–2333, https://doi.org/10.1007/s00382-011-1014-4, 2011.

Brasseur, G.: Aeronomy of the Middle Atmosphere : Chemistry and Physics of the Stratosphere and Mesosphere, Atmospheric sciences library ; 5, Springer Netherlands, 3rd edn., 2005.

Butler, A. H., Seidel, D. J., Hardiman, S. C., Butchart, N., Birner, T., and Match, A.: Defining Sudden Stratospheric Warmings, Bull. Amer. Meteor. Soc., 96, 1913–1928, 2015.

Byrne, N. J. and Shepherd, T. G.: Seasonal persistence of circulation anomalies in the Southern Hemisphere stratosphere, and its implications for the troposphere, Journal of Climate, 31, 3467–3483, https://doi.org/10.1175/jcli-d-17-0557.1, 2018.

Charlton, A. J. and Polvani, L. M.: A New Look at Stratospheric Sudden Warmings. Part I: Climatology and Modeling Benchmarks, J. Clim., 20, 449–469, https://doi.org/10.1175/JCLI3996.1, 2007.

Coy, L., Wargan, K., Molod, A. M., McCarty, W. R., and Pawson, S.: Structure and Dynamics of the Quasi-Biennial Oscillation in MERRA-2, J. Clim., 29, 5339–5354, https://doi.org/10.1175/JCLI-D-15-0809.1, https://doi.org/10.1175/JCLI-D-15-0809.1, 2016.

de la Cámara, A., Birner, T., and Albers, J. R.: Are Sudden Stratospheric Warmings Preceded by Anomalous Tropospheric Wave Activity?, Journal of Climate, 32, 7173 – 7189, https://doi.org/10.1175/jcli-d-19-0269.1, 2019.

Doddridge, E. W. and Marshall, J.: Modulation of the Seasonal Cycle of Antarctic Sea Ice Extent Related to the Southern Annular Mode, Geophys. Res. Lett., 44, 9761–9768, https://doi.org/10.1002/2017GL074319, 2017.

Domeisen, D. I. V., Butler, A. H., Perez, A. J. C., Ayarzagüena, B., Baldwin, M. P., Sigouin, E. D., Furtado, J. C., Garfinkel, C. I., Hitchcock, P., Karpechko, A. Y., Kim, H., Knight, J. R., Lang, A. L., Lim, E. P., Marshall, A., Roff, G., Schwartz, C., Simpson, I. R., Son, S.-W., and Taguchi, M.: The role of the stratosphere in subseasonal to seasonal prediction Part II: Predictability arising from stratosphere - troposphere coupling, J. Geophys. Res.: Atmos., 125, 2019JD030 923, https://doi.org/10.1029/2019JD030923, 2019a.

Domeisen, D. I. V., Garfinkel, C. I., and Butler, A. H.: The Teleconnection of El Niño Southern Oscillation to the Stratosphere, Rev. Geophys., 57, 5–47, https://doi.org/10.1029/2018RG000596, 2019b.

Domeisen, D. I. V., Butler, A. H., Perez, A. J. C., Ayarzagüena, B., Baldwin, M. P., Sigouin, E. D., Furtado, J. C., Garfinkel, C. I., Hitchcock, P., Karpechko, A. Y., Kim, H., Knight, J. R., Lang, A. L., Lim, E. P., Marshall, A., Roff, G., Schwartz, C., Simpson, I. R., Son, S.-W., and Taguchi, M.: The Role of the Stratosphere in Subseasonal to Seasonal Prediction: 1. Predictability of the Stratosphere, Journal of Geophysical Research: Atmospheres, 125, e2019JD030 920, https://doi.org/10.1029/2019jd030920, 2020.

Duck, T., Whiteway, J., and Carswell, A.: The Gravity Wave-Arctic Stratospheric Vortex Interaction, J. Atmos. Sci., https://doi.org/10.1175/1520-0469(2001)058<3581:TGWASV>2.0.CO;2, 2001.

Edmon, H. J., Hoskins, B. J., and McIntyre, M. E.: Eliassen-Palm Cross Sections for the Troposphere, J. Atmos. Sci., 37, 2600 – 2616, 1980.

Eswaraiah, S., Kim, Y. H., Hong, J., Kim, J.-H., Ratnam, M. V., Chandran, A., Rao, S., and Riggin, D.: Mesospheric signatures observed during 2010 minor stratospheric warming at King Sejong Station (62 °S, 59 °W), J. Atmos. Sol.-Ter. Phys., 140, 55 – 64, https://doi.org/10.1016/j.jastp.2016.02.007, 2016.

Eswaraiah, S., Kim, Y. H., Lee, J., Ratnam, M. V., and Rao, S. V. B.: Effect of Southern Hemisphere Sudden Stratospheric Warmings on Antarctica Mesospheric Tides: First Observational Study, J. Geophys. Res.: Space Physics, 123, 2127–2140, https://doi.org/10.1002/2017JA024839, 2018.

Eswaraiah, S., Kim, J.-H., Lee, W., Hwang, J., Kumar, K. N., and Kim, Y. H.: Unusual Changes in the Antarctic Middle Atmosphere During the 2019 Warming in the Southern Hemisphere, Geophys. Res. Lett., 47, e2020GL089 199, https://doi.org/10.1029/2020GL089199, 2020a.

Eswaraiah, S., Lee, C., Lee, W., Kim, Y. H., Kumar, K. N., and Medineni, V. R.: Temperature tele-connections between the tropical and polar middle atmosphere in the Southern Hemisphere during the 2010 minor sudden stratospheric warming, Atmospheric Science Letters, 22, e1010, https://doi.org/10.1002/asl.1010, 2020b.

Garcia, R. R., Dunkerton, T. J., Lieberman, R. S., and Vincent, R. A.: Climatology of the semiannual oscillation of the tropical middle atmosphere, J. Geophys. Res.: Atmos., 102, 26 019–26 032, https://doi.org/10.1029/97JD00207, 1997.

Gelaro, R., McCarty, W., Suárez, M. J., Todling, R., Molod, A., Takacs, L., Randles, C. A., Darmenov, A., Bosilovich, M. G., Reichle, R., Wargan, K., Coy, L., Cullather, R., Draper, C., Akella, S., Buchard, V., Conaty, A., Silva, A. M. D., Gu, W., Kim, G.-K., Koster, R., Lucchesi, R., Merkova, D., Nielsen, J. E., Partyka, G., Pawson, S., Putman, W., Rienecker, M., Schubert, S. D., Sienkiewicz, M., and Zhao, B.: The Modern-Era Retrospective Analysis for Research and Applications, Version 2 (MERRA-2), J. Clim., pp. 5419–5454, 2017.

Global Modeling and Assimilation Office (GMAO): MERRA-2 inst6_3d_ana_Np: 3d,6-Hourly,Instantaneous,Pressure-Level,Analysis,Analyzed Meteorological Fields V5.12.4, Greenbelt, MD, USA, Goddard Earth Sciences Data and Information Services Center (GES DISC), 10.5067/A7S6XP56VZWS, doi:0.5067/A7S6XP56VZWS, accessed 21 October 2020, 2015.

Gray, L.: The influence of the equatorial upper stratosphere on stratospheric sudden warmings, Geophys. Res. Lett., 30, 1166, https://doi.org/10.1029/2002GL016430, 2003.

Gray, L. J., Brown, M. J., Knight, J., Andrews, M., Lu, H., O'Reilly, C., and Anstey, J.: Forecasting extreme stratospheric polar vortex events, Nature Comm., 11, https://doi.org/10.1038/s41467-020-18299-7, 2020.

Holton, J. R.: An introduction to dynamic meteorology, Academic Press, 5th edn., 2012.

Holton, J. R. and Tan, H.-C.: The Influence of the Equatorial Quasi-Biennial Oscillation on the Global Circulation at 50 mb, J. Atmos. Sci., 37, 2200–2208, https://doi.org/10.1175/1520-0469(1980)037<2200:TIOTEQ>2.0.CO;2, 1980.

Hoppel, K., Bevilacqua, R., Allen, D., Nedoluha, G., and Randall, C.: POAM III observations of the anomalous 2002 Antarctic ozone hole, Geophys. Res. Lett., 30, 1394, https://doi.org/10.1029/2003GL016899, 2003.

Kanzawa, H. and Kawaguchi, S.: Large stratospheric sudden warming in Antarctic late winter and shallow ozone hole in 1988, Geophysical Research Letters, 17, 77–80, https://doi.org/10.1029/GL017i001p00077, 1990.

Kawatani, Y., Hirooka, T., Hamilton, K., Smith, A. K., and Fujiwara, M.: Representation of the equatorial stratopause semiannual oscillation in global atmospheric reanalyses, Atmos. Chem. Phys., 20, 9115–9133, https://doi.org/10.5194/acp-20-9115-2020, 2020.

Klekociuk, A., Tully, M., Krummel, P., Kravchenko, V., Henderson, S., Alexander, S., Querel, R., Nichol, S., Smale, D., Milinevsky, G., Grytsai, A., Fraser, P., Xiangdong, Z., Gies, H., Schofield, R., and Shanklin, J.: The Antarctic ozone hole during 2017, Journal of Southern Hemisphere Earth Systems Science, 69, 29–51, https://doi.org/10.1071/ES19019, 2020.

Kuai, L., Shia, R.-L., Jiang, X., Tung, K. K., and Yung, Y. L.: Nonstationary Synchronization of Equatorial QBO with SAO in Observations and a Model, J. Atmos. Sci., 66, 1654–1664, https://doi.org/10.1175/2008JAS2857.1, 2009.

Kwon, H., Choi, H., Kim, B.-M., Kim, S.-W., and Kim, S.-J.: Recent weakening of the southern stratospheric polar vortex and its impact on the surface climate over Antarctica, Environmental Research Letters, 15, 094 072, https://doi.org/10.1088/1748-9326/ab9d3d, 2020.

Labitzke, K.: On the solar cycle–QBO relationship: a summary, J. Atmos. Sol. Terr. Phys., 67, 45–54, https://doi.org/10.1016/j.jastp.2004.07.016, 2005.

Lawrence, Z. D. and Manney, G. L.: Does the Arctic Stratospheric Polar Vortex Exhibit Signs of Preconditioning Prior to Sudden Stratospheric Warmings?, J. Atmos. Sci., 77, 611–632, https://doi.org/10.1175/JAS-D-19-0168.1, 2020.

Lim, E.-P., Hendon, H. H., and Thompson, D. W. J.: Seasonal Evolution of Stratosphere-Troposphere Coupling in the Southern Hemisphere and Implications for the Predictability of Surface Climate, Journal of Geophysical Research: Atmospheres, 123, 12,002–12,016, https://doi.org/10.1029/2018JD029321, 2018.

Lim, E. P., Hendon, H. H., Boschat, G., Hudson, D., Thompson, D. W. J., Dowdy, A. J., and Arblaster, J. M.: Australian hot and dry extremes induced by weakenings of the stratospheric polar vortex, Nature Geosci., 12, 896–901, https://doi.org/10.1038/s41561-019-0456-x, 2019.

Madden–Julian oscillation index (MJO): https://www.cpc.ncep.noaa.gov/products/precip/CWlink/MJO/whindex.shtml, last accessed 24 May, 2021.

Manney, G. L., Livesey, N. J., Santee, M. L., Froidevaux, L., Lambert, A., Lawrence, Z. D., Millán, L. F., Neu, J. L., Read, W. G., Schwartz, M. J., and Fuller, R. A.: Record-Low Arctic Stratospheric Ozone in 2020: MLS Observations of Chemical Processes and Comparisons With Previous Extreme Winters, Geophys. Res. Lett., 47, 103, https://doi.org/10.1029/2020GL089063, 2020.

Matsuno, T.: A Dynamical Model of the Stratospheric Sudden Warming, Journal of Atmospheric Sciences, 28, 1479–1494, https://doi.org/10.1175/1520-0469(1971)028<1479:ADMOTS>2.0.CO;2, 1971.

Moss, A. C., Wright, C. J., Davis, R. N., and Mitchell, N. J.: Gravity-wave momentum fluxes in the mesosphere over Ascension Island (8°S, 14°W) and the anomalous zonal winds of the semi-annual oscillation in 2002, Ann. Geophys., 34, 323–330, https://doi.org/10.5194/angeo-34-323-2016, 2016.

Multivariate ENSO Index Version 2 (MEI.v2): https://psl.noaa.gov/enso/mei/, last accessed 3 Dec, 2020.

Pascoe, C. L., Gray, L. J., and Scaife, A. A.: A GCM study of the influence of equatorial winds on the timing of sudden stratospheric warmings, Geophys. Res. Lett., 33, L06 825, https://doi.org/10.1029/2005GL024715, 2006.

Peña-Ortiz, C., Schmidt, H., Giorgetta, M. A., and Keller, M.: QBO modulation of the semiannual oscillation in MAECHAM5 and HAMMONIA, J. Geophys. Res.: Atmos., 115, D21 106, https://doi.org/10.1029/2010JD013898, 2010.

Rao, J., Garfinkel, C. I., Chen, H., and White, I. P.: The 2019 New Year Stratospheric Sudden Warming and Its Real-Time Predictions in Multiple S2S Models, Journal of Geophysical Research: Atmospheres, 124, 11 155–11 174, https://doi.org/10.1029/2019jd030826, 2019.

Rao, J., Garfinkel, C. I., and White, I. P.: Predicting the Downward and Surface Influence of the February 2018 and January 2019 Sudden Stratospheric Warming Events in Subseasonal to Seasonal (S2S) Models, Journal of Geophysical Research: Atmospheres, 125, e2019JD031 919, https://doi.org/10.1029/2019jd031919, 2020a.

Rao, J., Garfinkel, C. I., and White, I. P.: How does the Quasi- Biennial Oscillation affect the boreal winter tropospheric circulation in CMIP5/6 models?, Journal of Climate, 33, 1–54, https://doi.org/10.1175/jcli-d-20-0024.1, 2020b.

Rao, J., Garfinkel, C. I., White, I. P., and Schwartz, C.: The Southern Hemisphere Minor Sudden Stratospheric Warming in September 2019 and its Predictions in S2S Models, J. Geophys. Res.: Atmos., 125, e2020JD032 723, https://doi.org/10.1029/2020JD032723, 2020c.

Ricaud, P., Lefèvre, F., Berthet, G., Murtagh, D., Llewellyn, E. J., Mégie, G., Kyrölä, E., Leppelmeier, G. W., Auvinen, H., Boonne, C., Brohede, S., Degenstein, D. A., de La Noë, J., Dupuy, E., El Amraoui, L., Eriksson, P., Evans, W. F. J., Frisk, U., Gattinger, R. L., Girod, F., Haley, C. S., Hassinen, S., Hauchecorne, A., Jimenez, C., Kyrö, E., Lautié, N., Le Flochmoën, E., Lloyd, N. D., McConnell, J. C., McDade, I. C., Nordh, L., Olberg, M., Pazmino, A., Petelina, S. V., Sandqvist, A., Seppälä, A., Sioris, C. E., Solheim, B. H., Stegman, J., Strong, K., Taalas, P., Urban, J., von Savigny, C., von Scheele, F., and Witt, G.: Polar vortex evolution during the 2002 Antarctic major warming as observed by the Odin satellite, J. Geophys. Res.: Atmos., 110, D05 302, https://doi.org/10.1029/2004JD005018, 2005.

Richter, J. H., Matthes, K., Calvo, N., and Gray, L. J.: Influence of the quasi-biennial oscillation and El Niño–Southern Oscillation on the frequency of sudden stratospheric warmings, J. Geophys. Res.: Atmos., 116, D20 111, https://doi.org/10.1029/2011JD015757, 2011.

Schoeberl, M. and Newman, P.: Encyclopedia of Atmospheric Sciences: Second Edition, chap. Middle Atmosphere: Polar Vortex, pp. 12–17, Schoeberl, M.R. and Newman, P.A., 2014.

Schoeberl, M. R., Stolarski, R. S., and Krueger, A. J.: The 1988 Antarctic ozone depletion: Comparison with previous year depletions, Geophysical Research Letters, 16, 377–380, https://doi.org/https://doi.org/10.1029/GL016i005p00377, 1989.

Schwartz, C. and Garfinkel, C. I.: Relative roles of the MJO and stratospheric variability in North Atlantic and European winter climate, Journal of Geophysical Research: Atmospheres, 122, 4184–4201, https://doi.org/10.1002/2016JD025829, 2017.

Shen, X., Wang, L., and Osprey, S.: The Southern Hemisphere sudden stratospheric warming of September 2019, Science Bulletin, 65, 1800–1802, https://doi.org/10.1016/j.scib.2020.06.028, 2020.

Smith, A. K., Garcia, R. R., Moss, A. C., and Mitchell, N. J.: The Semiannual Oscillation of the Tropical Zonal Wind in the Middle Atmosphere Derived from Satellite Geopotential Height Retrievals, Journal of the Atmospheric Sciences, 74, 2413–2425, https://doi.org/10.1175/jas-d-17-0067.1, 2017.

Smith, A. K., Holt, L. A., Garcia, R. R., Anstey, J. A., Serva, F., Butchart, N., Osprey, S., Bushell, A. C., Kawatani, Y., Kim, Y.-H., Lott, F., Braesicke, P., Cagnazzo, C., Chen, C.-C., Chun, H.-Y., Gray, L., Kerzenmacher, T., Naoe, H., Richter, J., Versick, S., Schenzinger, V., Watanabe, S., and Yoshida, K.: The equatorial stratospheric semiannual oscillation and time-mean winds in QBOi models, Q. J. R. Meteorol. Soc., pp. 1–17, https://doi.org/10.1002/qj.3690, 2020.

Solomon, S.: Stratospheric ozone depletion: A review of concepts and history, Rev. Geophys., 37, 275–316, https://doi.org/10.1029/1999RG900008, 1999.

Solomon, S., Garcia, R. R., Rowland, F. S., and Wuebbles, D. J.: On the depletion of Antarctic ozone, Nature, 321, 755–758, https://doi.org/10.1038/321755a0, 1986.

Taguchi, M. and Hartmann, D. L.: Interference of extratropical surface climate anomalies induced by El Niño and stratospheric sudden warmings, Geophys. Res. Lett., 32, L04 709, https://doi.org/10.1029/2004GL022004, 2005.

Thompson, D. W. J., Baldwin, M. P., and Solomon, S.: Stratosphere–Troposphere Coupling in the Southern Hemisphere, Journal of the Atmospheric Sciences, 62, 708–715, https://doi.org/10.1175/jas-3321.1, 2005.

Volland, H.: Atmospheric Tidal and Planetary Waves, Springer Netherlands, 1988.

Watson, P. A. G. and Gray, L. J.: How does the quasi-biennial oscillation affect the stratospheric polar vortex?, J. Atmos. Sci., 71, 391–409, https://doi.org/10.1175/JAS-D-13-096.1, 2014.

Wheeler, M. C. and Hendon, H. H.: An All-Season Real-Time Multivariate MJO Index: Development of an Index for Monitoring and Prediction, Monthly Weather Review, 132, 1917–1932, https://doi.org/10.1175/1520-0493(2004)132<1917:AARMMI>2.0.CO;2, 2004.

Wohltmann, I., von der Gathen, P., Lehmann, R., Maturilli, M., Deckelmann, H., Manney, G. L., Davies, J., Tarasick, D., Jepsen, N., Kivi, R., Lyall, N., and Rex, M.: Near-Complete Local Reduction of Arctic Stratospheric Ozone by Severe Chemical Loss in Spring 2020, Geophys. Res. Lett., 47, 42, https://doi.org/10.1029/2020GL089547, 2020.

Yamazaki, Y., Matthias, V., Miyoshi, Y., Stolle, C., Siddiqui, T., Kervalishvili, G., Laštovička, J., Kozubek, M., Ward, W., Themens, D. R., Kristoffersen, S., and Alken, P.: September 2019 Antarctic Sudden Stratospheric Warming: Quasi-6-Day Wave Burst and Ionospheric Effects, Geophys. Res. Lett., 47, e2019GL086 577, https://doi.org/10.1029/2019GL086577, 2020.

Zhang, T., Hoell, A., Perlwitz, J., Eischeid, J., Murray, D., Hoerling, M., and Hamill, T. M.: Towards Probabilistic Multivariate ENSO Monitoring, Geophys. Res. Lett., 46, 10 532–10 540, https://doi.org/10.1029/2019GL083946, 2019.

MERRA-2 geopotential height maps for 2 hPa pressure level over Antarctica for selected dates during winter 2019. Low geopotential heights indicate the position of the polar vortex. Latitude circles are shown at 10° intervals and longitudinal sectors are shown at 40° intervals. Dates shown in individual panels are (a) June 25, 2019, (b) July 17, (c) August 26, (d) September 13.

As Figure **??** but for the 40 hPa pressure level.

As Figure **??** but averaged over 1993, 1995, 1997 and 1999. Time periods for the 7 day averages as given in the figure titles.

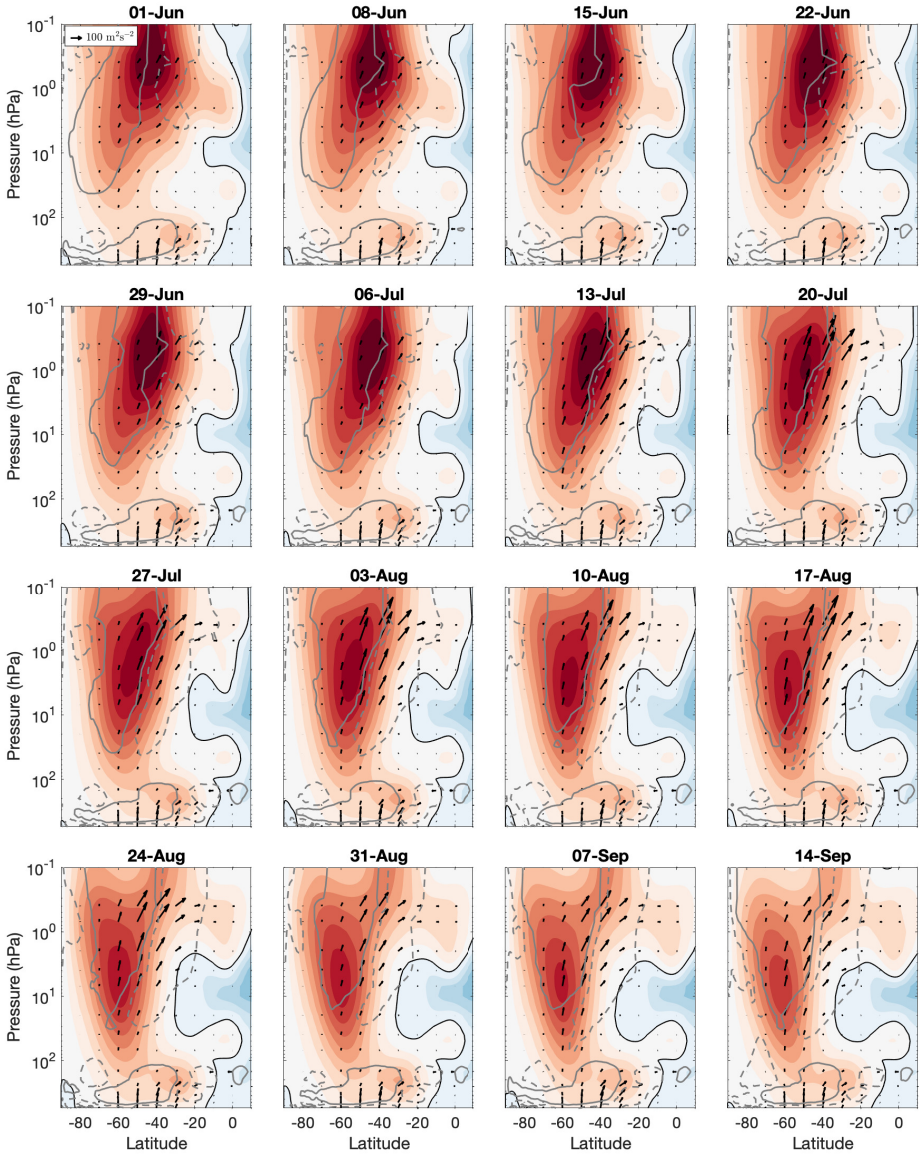


**Figure 1.** ~~7-day~~ 7-day average zonal mean zonal wind (~~filled~~ contours, interval 10 $ms^{-1}$)~~and~~ , Eliassen-Palm (EP) flux (arrows, $m^2s^{-2}$, reference arrow shown in first panel) and EP flux divergence ($\pm 2$ $ms^{-1}day^{-1}$, convergence indicated by dashed grey lines, divergence indicated by solid grey lines) for the ~~austral winter~~ reference eQBO years (excluding 1988, 2002, 2017 and 2019~~from MERRA-2~~). Each figure covers the latitudinal range of 90°S to ~~90~~10°N and the vertical range of 550 hPa to 0.1 hPa. The ~~time periods (exact dates as given in figure titles) shown have been selected to depict the evolution of the events. Note that the time periods encompass those shown in Figure ??. EP flux convergence is indicated with dashed line. The~~ solid ~~white~~ black line shows the location of the zero wind line. First day of averaging in each figure is given in the title.

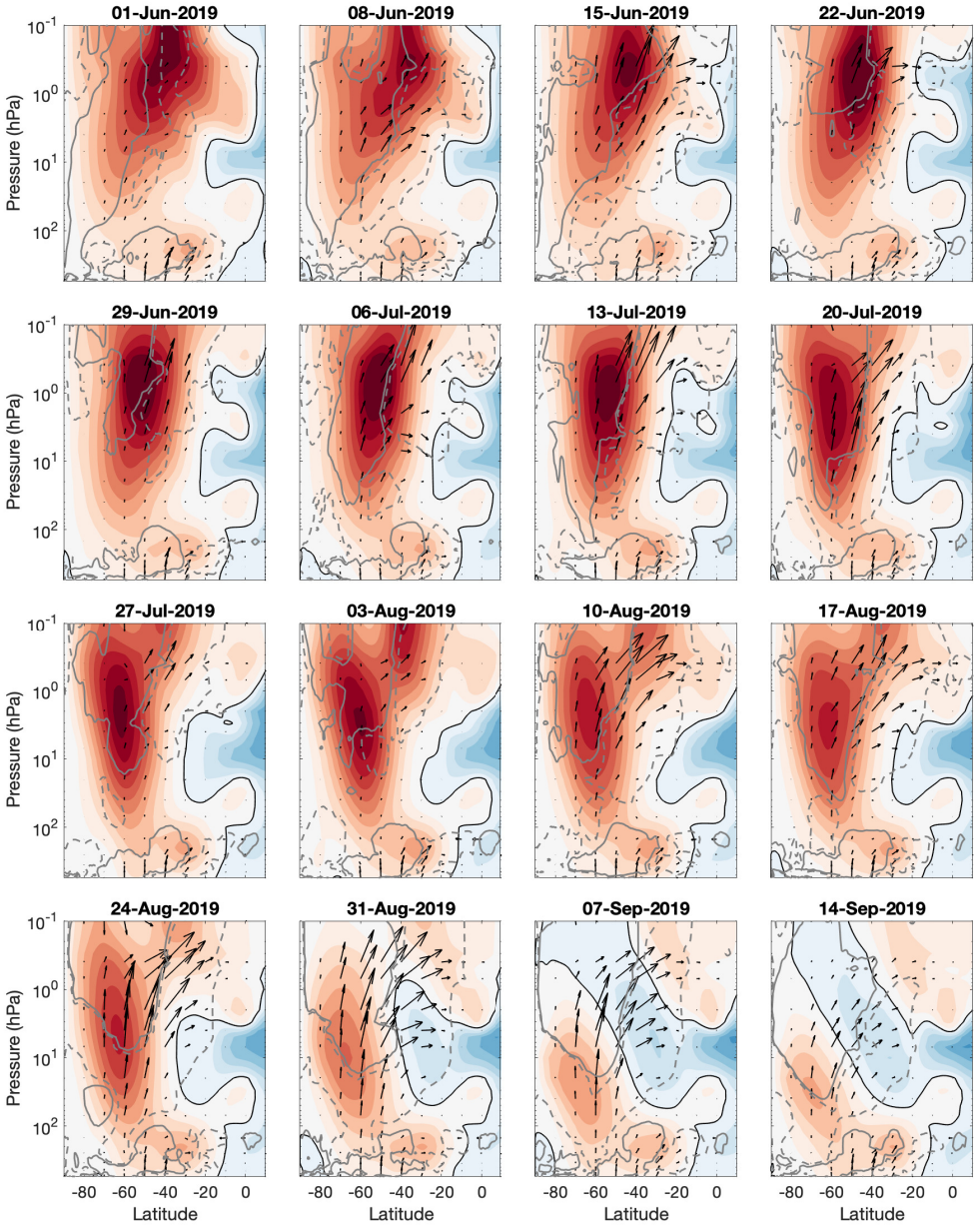


**Figure 2.** ~~The same as~~ As Figure ~~??~~ ~~(d),~~ 1 but for the ~~zonal averaging in EP flux calculation according to equations (1) and (2) has now been made over the longitudinal sectors (clockwise) (a) 40°E-140°W and (b) 140°W-40°E .~~year 2019.

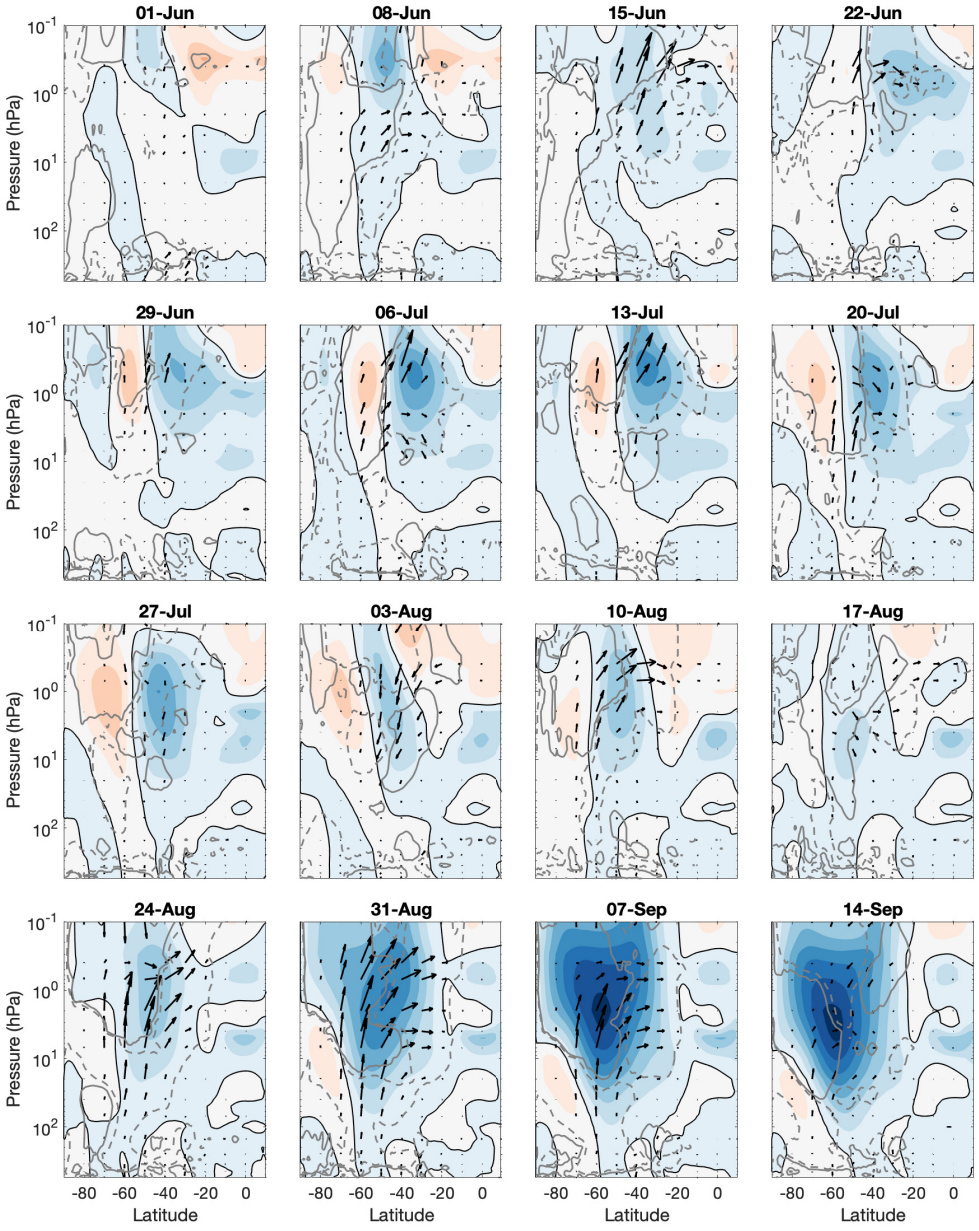


**Figure 3.** ~~Temporal evolution (June 1 to July 31,~~ Anomaly: 2019 ~~) of the zonal mean zonal~~ - reference eQBO years. Zonal wind ~~(ms$^{-1}$)~~ anomaly contours, EP-flux vectors and divEP levels as in ~~the vertical range of 100~~Figure ~~hPa to 0.1 hPa, averaged between 15-20°S~~1.~~The white line signifies the zero wind line.~~

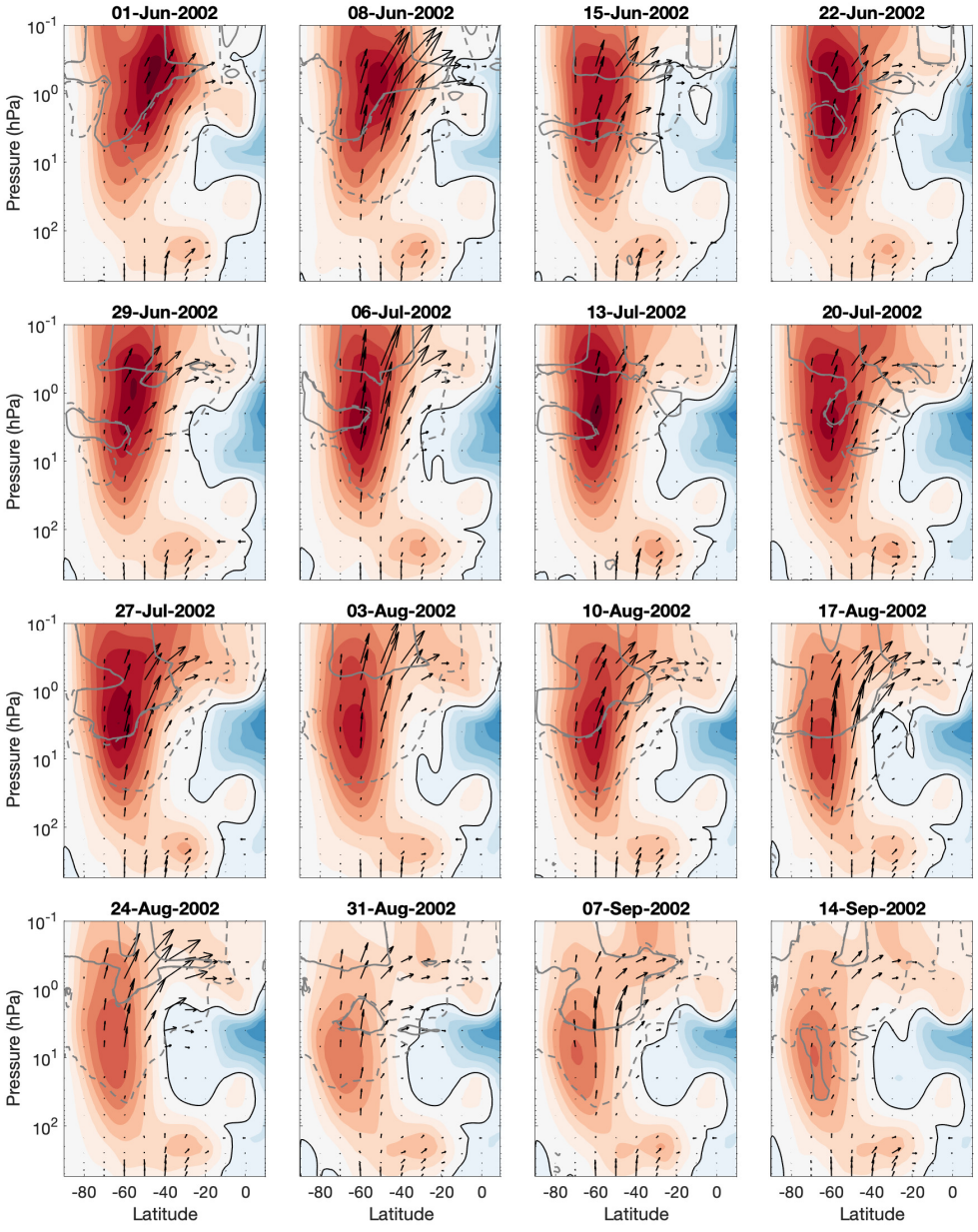


**Figure 4.** As Figure ~~??~~ 1 but for the year 2002.~~The time periods (exact dates as given in figure titles) shown have been selected to depict the evolution of the events. Panel (d) corresponds to the SSW and vortex split event.~~

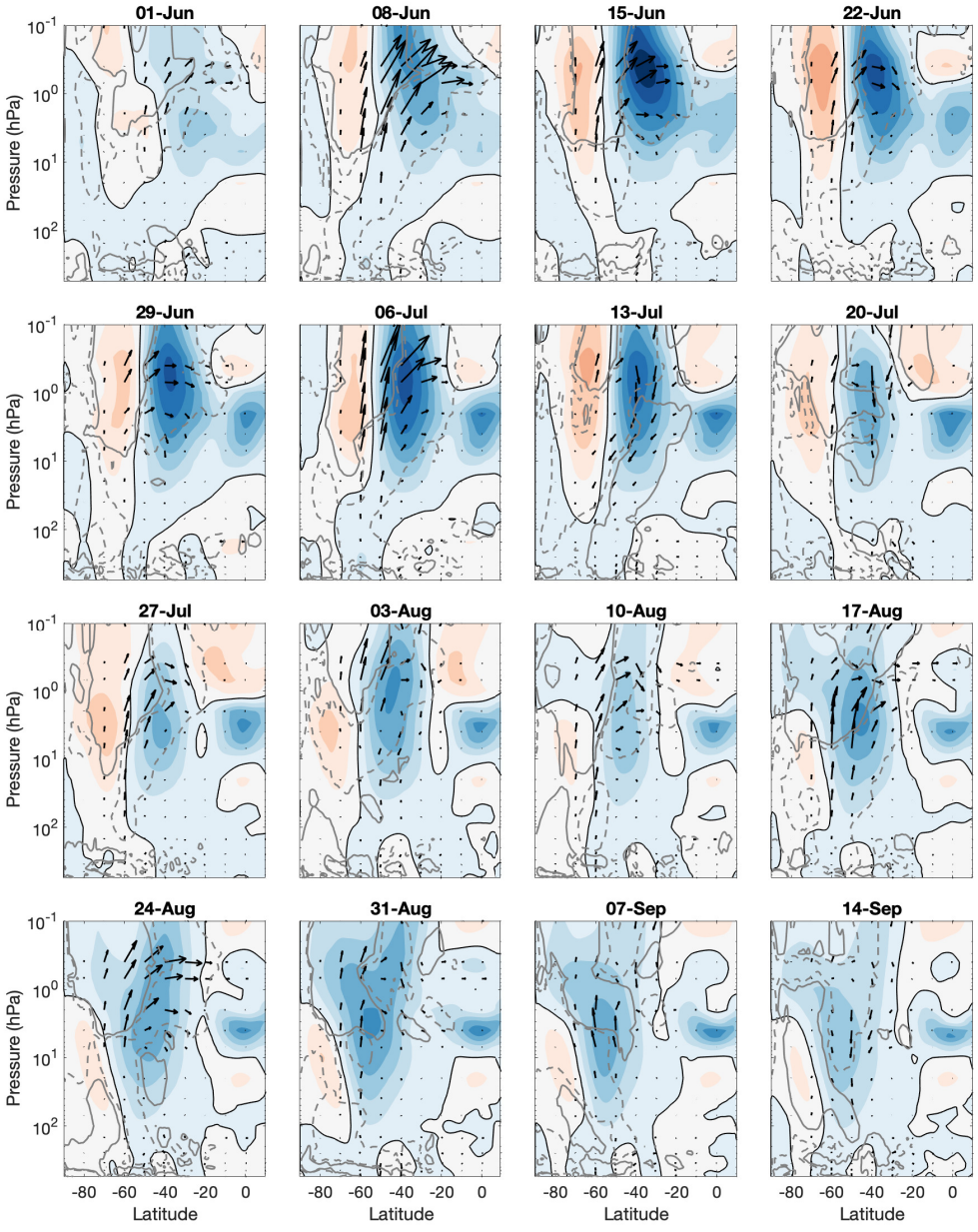


**Figure 5.** As Figure ~~??,~~ 3 but now showing the anomaly for the year ~~2002 -~~ 2002.

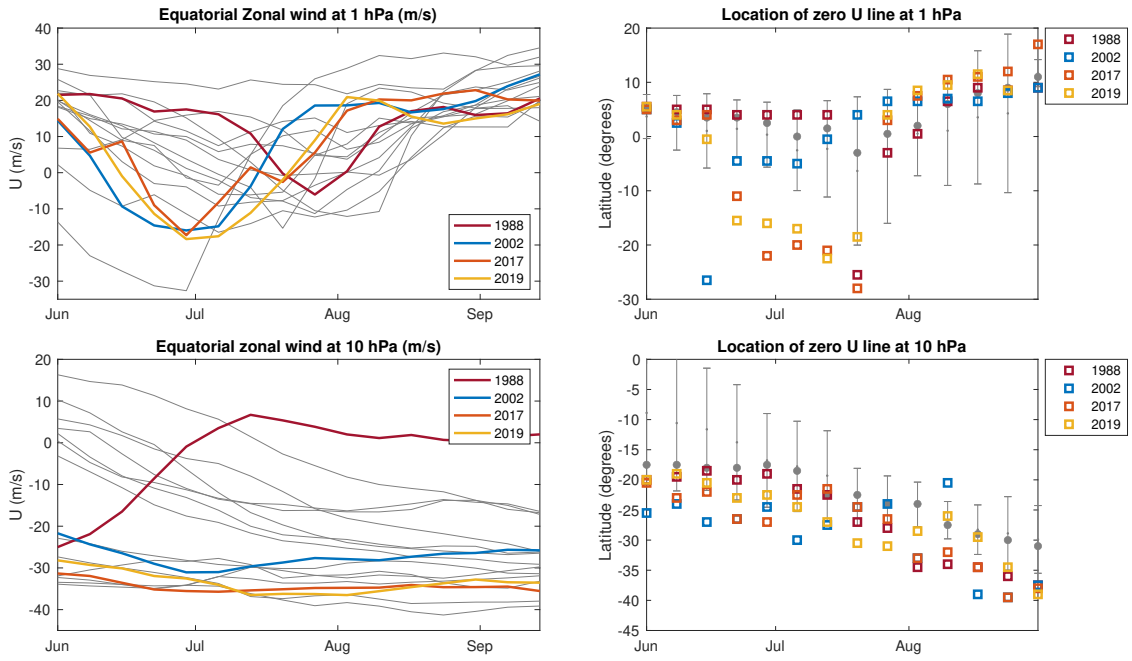


**Figure 6.** ~~As Figure ?? but for~~ Top (left): Evolution of the ~~year 2017. The time periods~~ equatorial (~~exact dates as given in figure titles~~5°S-5°N) ~~shown have been selected~~ SAO zonal wind at 1 hPa level ($ms^{-1}$) from June to ~~depict~~ September. The grey lines show the ~~evolution~~ wind for all eQBO years with the years 1988, 2002, 2017, and 2019 highlighted with red, blue, orange, and yellow lines, respectively. Top (right) Latitudinal location of the ~~events~~zero zonal wind line at 1 hPa level. The small grey dot indicates the mean location while the large grey circle indicates the median location during the eQBO years. For clarity, the grey bars show the $1 \times \sigma$ deviation around the mean location. Years 1988, 2002, 2017, and 2019 are highlighted with red, blue, orange, and yellow markers, respectively. Bottom: As above, but for the zonal wind at the 10 hPa level for QBO.

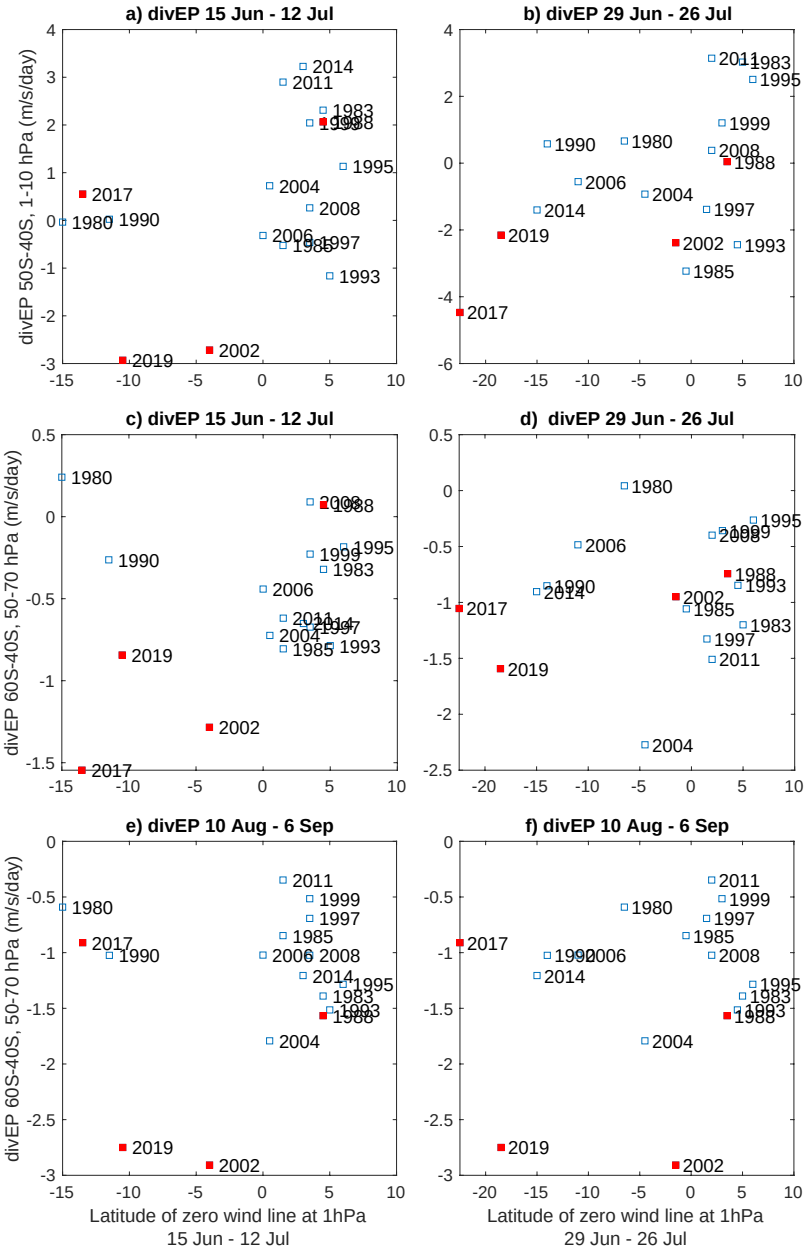


**Figure 7.** ~~As Figure~~Latitude of the zero wind line (x-axis) at 1 ~~?? but averaged over 1980~~hPa level (left panels: 15 June – 12 July; right panels: 29 June – 26 July) versus EP flux divergence (divEP, ~~1983~~$ms^{-1}day^{-1}$, ~~1985~~ y-axis). a-b) Mean EP flux divergence at 50°S-40°S and ~~1990. Time periods for~~ between 1-10 hPa, times as given in the ~~7 day averages~~ titles; c-f) Mean EP flux divergence at 60°S-40°S and between 50-70 hPa, times as given in the ~~figure~~ titles.

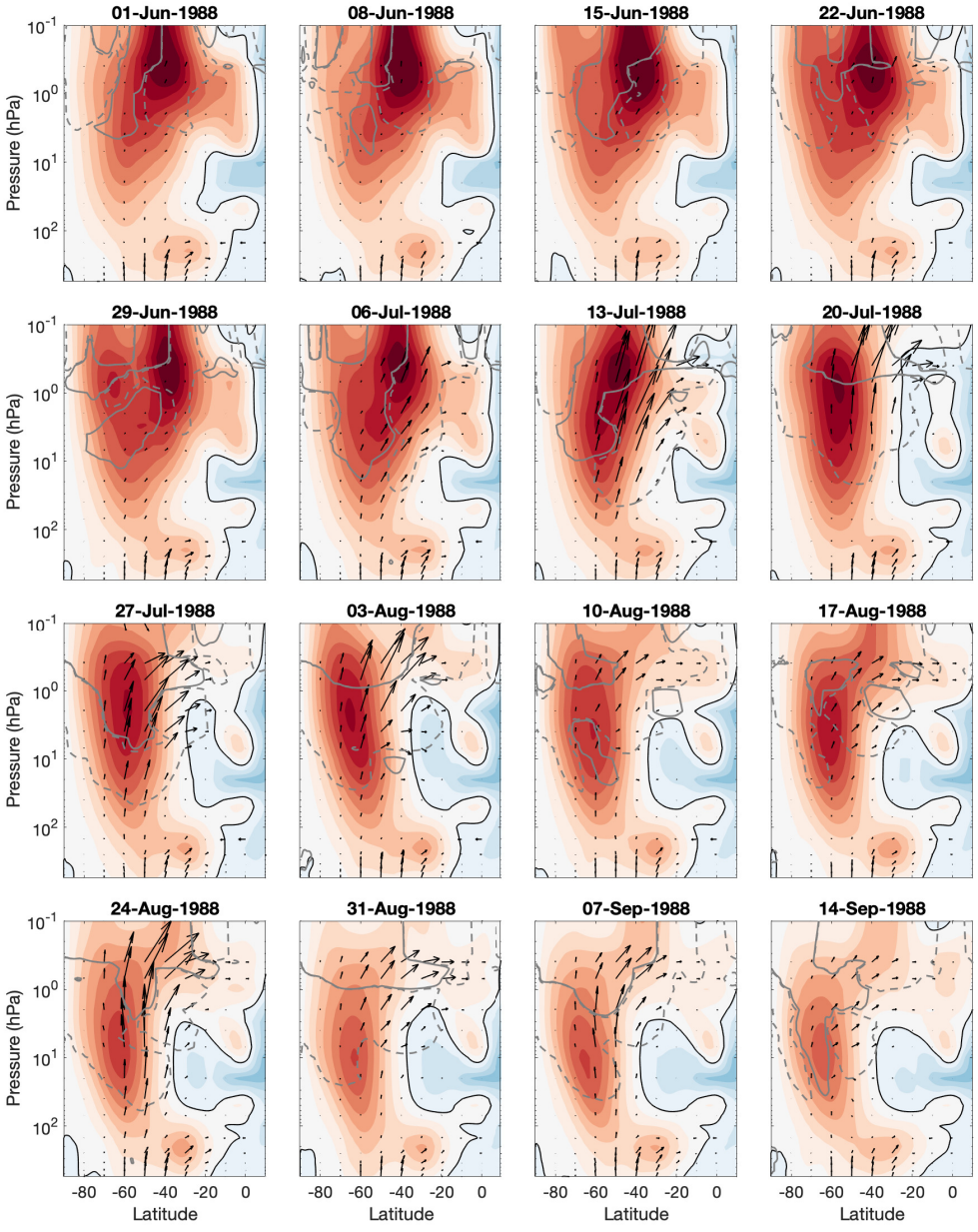


**Figure 8.** Supplement: As Figure ~~??~~ 1 but ~~averaged over 2004, 2006 and 2008. Time periods~~ for the ~~7 day averages as given in the figure titles.~~ year 1988.

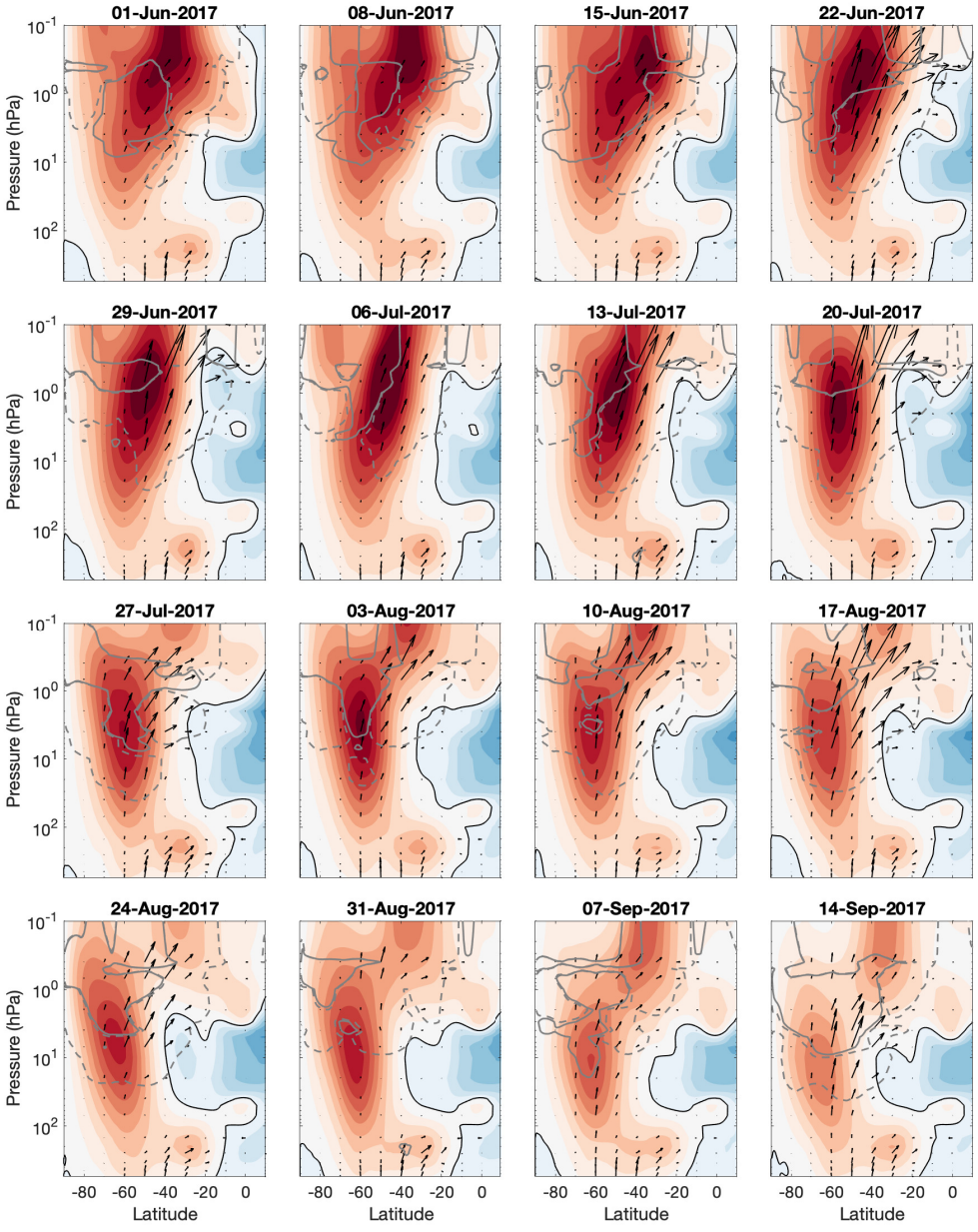


**Figure 9.** Supplement: As Figure ~~??~~ 1 but ~~averaged over 2011 and 2014. Time periods~~ for the ~~7 day averages as given in the figure titles.~~ year 2017.